Draft version February 25, 2013
Preprint typeset using LaTeX style emulateapj v. 5/2/11

arXiv:1203.1618v1 [astro-ph.SR] 7 Mar 2012

HOW GOOD OF A CLOCK IS ROTATION? THE STELLAR ROTATION-MASS-AGE RELATIONSHIP FOR OLD FIELD STARS

Courtney R. Epstein[1] and Marc H. Pinsonneault[1]

Draft version February 25, 2013

ABSTRACT

The rotation-mass-age relationship offers a promising avenue for measuring the ages of field stars, assuming the attendant uncertainties to this technique can be well characterized. We model stellar angular momentum evolution starting with a rotation distribution from open cluster M37. Our predicted rotation-mass-age relationship shows significant zero-point offsets compared to an alternative angular momentum loss law and published gyrochronology relations. Systematic errors at the 30 percent level are permitted by current data, highlighting the need for empirical guidance. We identify two fundamental sources of uncertainty that limit the precision of rotation-based ages and quantify their impact. Stars are born with a range of rotation rates, which leads to an age range at fixed rotation period. We find that the inherent ambiguity from the initial conditions is important for all young stars, but becomes large for old stars below 0.6 $M_\odot$. Latitudinal surface differential rotation also introduces a minimum uncertainty into rotation period measurements and, by extension, rotation-based ages. Both models and the data from binary star systems 61 Cyg and α Cen demonstrate that latitudinal differential rotation is the limiting factor for rotation-based age precision among old field stars, inducing uncertainties at the ~ 2 Gyr level. We also examine the relationship between variability amplitude, rotation period, and age. Existing ground-based surveys can detect field populations with ages as old as $1-2$ Gyr, while space missions can detect stars as old as the Galactic disk. In comparison with other techniques for measuring the ages of lower main sequence stars, including geometric parallax and asteroseismology, rotation-based ages have the potential to be the most precise chronometer for $0.6-1.0$ $M_\odot$ stars.

Subject headings: Stars: evolution – Stars: rotation – Stars: late-type

1. INTRODUCTION

Ages of stars are both fundamental and difficult to measure. Stars of known age, such as members of star clusters, have therefore been studied intensively. For the far more numerous field stars, by contrast, our tools for inferring ages are blunt and inexact. We can infer ages for some binary stars, and also for turnoff stars, from the combination of parallax and metallicity measurements. However, for typical M–G dwarfs, slow luminosity evolution on the main sequence and ambiguities from metallicity and helium errors result in uncertain age estimates. Rotation provides an attractive alternative chronometer (e.g. Lachaume et al. 1999; Barnes 2007). Stars with minimal *nuclear* evolution can experience strong *rotational* evolution, in the sense that low mass stars are observed to rotate more slowly as they age. The idea of rotation as a clock for low mass stars is an old one; however, the prospect of rotation as a *precise* clock is new. We identify two effects that limit the intrinsic precision of rotation-age relationships: the large initial range of stellar rotation rates and surface differential rotation. We dedicate this paper to a comparison of rotation-mass-age predictions and a critical evaluation of the limiting precision of the rotation-mass-age relationship.

1.1. *A Standard Picture of Angular Momentum Loss in Low Mass Stars*

Measurements of Ca H and K emission for main sequence stars led Wilson (1963) to insightfully notice an inverse relationship between chromospheric activity and stellar age. In an influential paper, Skumanich (1972) argued that stellar rotation, activity, and lithium abundances for solar-like stars all decrease as the square root of age. Further progress was hindered by basic observational and theoretical limitations.

The theory of angular momentum evolution is complex. To predict rotation-age relationships, one must understand the origin of stellar rotation, angular momentum transport in stellar interiors, and angular momentum loss from magnetized solar-like winds. From an observational point of view, it is difficult to measure rotation periods in old field stars from either photometric or spectroscopic methods. This difficulty has been amplified by the even smaller subset of stars with independent age estimates. A brief summary of the lessons learned is useful for placing ages inferred from rotation into the modern context.

Open clusters and star forming regions have been crucial for developing the standard picture of angular momentum evolution in low mass stars. Large rotation datasets, and models capable of addressing them, became available in the late 1980s (Stauffer et al. 1989; Pinsonneault et al. 1989). T Tauri stars represent the initial hydrostatic evolutionary stage for stars, and rotation measurements in star forming regions therefore set the initial conditions for angular momentum evolution. Open clusters provide snapshots in time of the evolution of stellar rotation rates. The simplest model of angular momentum evolution would begin with the distribution

---

[1] Department of Astronomy, Ohio State University, 140 W. 18th Ave., Columbus, OH 43210, USA; epstein,pinsono@astronomy.ohio-state.edu

of rotation rates in protostars and evolve them forward assuming solid body rotation and a scaled solar angular momentum loss rate $\mathrm{d}J/\mathrm{d}t \simeq \omega^3$ (Kawaler 1988), which reproduces the Skumanich law. Nature is not obliged to conform to such an idealized formula, however, and the obstacles to a more complete theoretical description are severe. Empirical guidance is thus essential.

A standard working model of angular momentum evolution has emerged, with some important refinements on the simplest possible model. Protostars of the same mass are born with a range of rotation rates (e.g. Bouvier et al. 1986; for more recent work see Rebull et al. 2004, Henderson & Stassun 2011). Early models starting in the protostellar regime (Pinsonneault et al. 1990) predicted that stars would converge to a narrow mass-rotation relationship at fixed age, but did not correctly predict the existence of either the most rapid or the slowest rotating stars in young open clusters. Three important refinements were introduced to explain the observed angular momentum evolution pattern.

The survival of rapid rotation in young stars prohibits a simple scaling of the solar torque by the cube of the rotation rate; saturation in the loss rate is required. A similar behavior is observed in proxies of magnetic activity (Noyes et al. 1984; Pizzolato et al. 2003) and expected in wind models (MacGregor & Brenner 1991). Both the activity and spin down data require a mass dependent saturation threshold (Sills et al. 2000), in the sense that lower mass stars saturate at lower rotation rates.

The opposite problem occurs for the slowest rotation rates seen in young open clusters; scaled solar winds are too inefficient to reach such low rotation rates so quickly. This led to the hypothesis of disk-locking (Koenigl 1991; Shu et al. 1994), which is the hypothesized rotational coupling between the stars convective envelope and the inner accretion disk. Observations require the existence of a net torque in excess of that expected from solar-like winds, and that this effect is more important for some stars than others. Characteristic lifetimes of order 6 Myr and less are observationally plausible for gaseous disk lifetimes (Haisch et al. 2001; but see also Mamajek 2009), and they can reconcile the protostellar and ZAMS rotation distributions (Tinker et al. 2002).

The final observational effect is the detection of core-envelope decoupling. Stars spin up as they contract onto the main sequence, where their structure stabilizes and the timescale for evolution increases. A magnetized wind will initially spin down the convective envelope; the radiative core will then respond over the internal angular momentum transport timescale. There will be a rapid initial drop in surface rotation if the transport timescale is long enough, followed by an epoch where the core spins down and the envelope does not (e.g. Endal & Sofia 1979). Once the entire star is coupled it will spin down as a solid body, even if there is a differentially rotating internal profile (Pinsonneault et al. 1989). The observational signature is that the slow rotator population in young open clusters spins down quickly at first, and then the spin down stalls. Numerous studies have confirmed this phenomenon (Keppens et al. 1995; Krishnamurthi et al. 1998; Allain 1998; Irwin et al. 2007b; Denissenkov et al. 2010), with inferred timescales in the range of tens to hundreds of Myr, depending on mass. The upper envelope of the rotation distribution appears to always spin down as a solid body, suggesting that the transport timescale is a function of both rotation rate and mass (Denissenkov et al. 2010). The underlying mechanisms for all three of these effects are active research topics, but they are all physically well-motivated and supported by strong empirical evidence. A practical consequence is that there are documented problems with adopting a Skumanich-style spin down model in young stars.

1.2. *Rotation Data and Gyrochronology*

The complex physical picture for young stars is daunting. Fortunately, there has been an explosion in the quality and quantity of stellar rotation data. This has largely been driven by planet transit searches, but dedicated stellar rotation programs, such as the Monitor Project, have also been valuable (Irwin et al. 2006, 2007a,b, 2008a,b and Meibom et al. 2009, 2011a,b). Stellar rotation periods are now available for bulk stellar populations, especially for cool and rapidly rotating stars. Space missions have extended our precision in both amplitude and period, raising the prospect of accurate rotation periods, even for old Sun-like stars (Basri et al. 2010). The qualitative rotation-mass-age relationships from earlier decades are now being re-evaluated as practical tools for stellar population studies, and open cluster stars have once again become a central calibrating tool. Modern rotation-mass-age, or gyrochronology, relations (Pace & Pasquini 2004; Barnes 2007; Mamajek & Hillenbrand 2008; Meibom et al. 2009, 2011a) are based on the following major insights gleaned from open cluster studies.

Young open clusters reveal that coeval stars of the same mass are born with a range of rotation rates (e.g. NGC 6530, Henderson & Stassun 2011; Orion Nebula Cluster, Attridge & Herbst 1992; IC 348, Herbst et al. 2000). However, the majority of young stars arrive on the main sequence as slow rotators (Stauffer et al. 1989 and Hartman et al. 2010 are nice examples for the Pleiades cluster.) One can therefore define a median relationship, even in young systems, which includes many of the stars. The width of the rotation distribution also narrows with time; this process is fastest for solar analogs and takes progressively longer for lower mass stars. This convergence is seen in solar analogs by ages of order 500 − 600 Myr, exemplified by the Hyades (Radick et al. 1987) and M37 (Hartman et al. 2009). Finally, the median rotation period at fixed color increases with increased age. Published gyrochronology prescriptions take advantage of these basic features to define working relationships between rotation, color, and age using a semi-empirical approach. The median rotation of the bulk population is defined for young open clusters, tested in clusters with ages under 1 Gyr, and extrapolated to older stars using the solar calibration as a constraint. Barnes (2007) suggested that the influence of color (mass) and age are independent effects and thus mathematically separable into two functions as shown below:

$$P(B-V,t) = f(B-V)g(t) \tag{1}$$

$$f(B-V) = a[(B-V)_0 - c]^b \tag{2}$$

$$g(t) = t^n \tag{3}$$

where the age t is in Myr. Spin down is accomplished with a power law $g(t)$ and an index of $n = 0.5$ corre-

TABLE 1
Parameters in Gyrochronology Models

Source	a	b	c	n
Barnes (2007)	0.7725 ± 0.011	0.601 ± 0.024	0.40	0.5189 ± 0.0070
Mamajek & Hillenbrand (2008)	0.407 ± 0.021	0.325 ± 0.024	0.495 ± 0.010	0.566 ± 0.008
Meibom et al. (2009)	0.770 ± 0.005	0.472 ± 0.027	0.553 ± 0.052	0.52

sponds to the Skumanich (1972) law. The polynomial $f(t)$ models the color dependence of the slow rotator sequence at fixed age. Since $f(B-V)$ lacks time dependence, any relationship of this form produces self-similar mass-rotation isochrones. Although many variations exist, for the purposes of this paper, we compare three published gyrochronology relationships, with parameters listed in Table 1. These gyrochronology relationships are typically calibrated to cluster data in the color range $0.5 \lesssim (\mathrm{B}-\mathrm{V})_0 \lesssim 1.4$. Both Barnes (2007) and Mamajek & Hillenbrand (2008) base the color-rotation relationship on many well studied clusters (e.g. α Per, the Pleiades, Hyades, etc.) and determine the index n as the factor that reproduces the Sun's rotation rate at the solar color. Meibom et al. (2009) fit the color dependence in a single cluster (M35), but retained the power law index n from Barnes (2007).

Gyrochronology is a promising concept, but there is real tension between our understanding of angular momentum evolution, cluster data, and a simple mapping of rotation onto a mass-dependent age. This is especially true for rotation-mass-age relationships in the context of young clusters, which we examine in a companion paper (Epstein, Pinsonneault, & Terndrup 2012; Paper II.) Fortunately, there is strong evidence that the physical picture is simpler for the older stars that will dominate a field sample. Protostar-accretion disk interactions are important on timescales of millions of years, while effective core-envelope coupling is established by an age of 500 Myr (e.g. Denissenkov et al. 2010). The bulk of the well-studied open cluster systems are clustered in age around the Pleiades (125 Myr) and Hyades (625 Myr), with a few systems in between.

In this paper, we therefore focus on the expected behavior of old field stars, with an emphasis on stars older than 500 Myr. The distribution of initial conditions can be empirically specified by open cluster stars, and the assumption of solid body spin down at this age and beyond is well-justified. Furthermore, there are good constraints on angular momentum loss, permitting a well-posed forward modeling of angular momentum evolution.

Much recent work has focused on presenting gyrochronology recipes as a function of color. We compare these relationships with angular momentum loss models and the extremely limited current data for old stars. New data, especially from the Kepler mission, will shed valuable light on the actual functional form of rotational evolution in old stars (a point that we will return to in the conclusions.) Here, we emphasize an under-appreciated aspect of the problem: *how precise are rotational ages?* For the purposes of this question, we assume that the mean rotation-mass-age relationship may be sufficiently well calibrated in the future such that its uncertainty is not the limiting factor in the error budget. Instead, we investigate the irreducible sources of uncertainty in rotation-based age measurements. In particular, both the initial scatter in stellar rotation and error in rotation period measurements place fundamental limits on rotation-based age measurements for old field stars.

This paper is organized as follows. Section 2 contains a detailed description of the initial conditions, stellar interior model, braking law, and assumptions necessary to model stellar angular momentum evolution. We present our results in §3. We compare the median rotation-mass-age relationship predicted by our preferred angular momentum loss model with an alternate braking law (§3.1.1) and published gyrochronology relations (§3.1.2). Those theoretical predictions are tested against observational constraints from two binary star systems 61 Cyg and α Cen in §3.1.3. Sources of uncertainty in obtaining rotation-based ages are quantified in §3.2. These include both fundamental limitations (e.g. arising from the initial scatter in rotation rates, §3.2.1, and from surface differential rotation, §3.2.2) and model-specific errors (§3.2.3–3.2.6).

Kepler and CoRoT are measuring asteroseismic ages for tens of thousands of old solar-like stars (e.g. Mosser et al. 2010; Gilliland et al. 2010). However, such space missions cover only a limited number of fields and targets. We therefore also examine how the prospects for rotation-mass-age relationships depend on the sensitivity of the survey. In §3.3, we demonstrate that ground-based studies can find young to intermediate aged populations (based on variability) for plausible precision ranges, while it is likely that the detection of older populations will require a degree of precision currently achievable only from space. Finally, in §4 we compare the limiting precision of rotation-based ages with other age diagnostics: trigonometric parallaxes and asteroseismology.

2. METHOD

Because of the paucity of data at old ages, we rely on the existing theoretical framework to predict the behavior of the rotation-mass-age relationship at late times. As described in §1.1, observations of rotation in open clusters (≤ 1 Gyr old) have guided theory to a standard model of angular momentum evolution. We treat the time evolution of rotation as an initial value problem. The initial mass-rotation distribution for our models is empirically determined by measurements of the populous open cluster M37 (550 Myr; Hartman et al. 2009.) Stellar angular momentum evolution is modeled with solid body angular momentum transport and a braking law specifying the torque provided by a stellar wind acting on a star. We compare two prescriptions for the strength of the wind: the commonly-used modified Kawaler law (Kawaler 1988; Sills et al. 2000) and the recently formulated loss law by Reiners & Mohanty (2012). These rotational evolution models piggyback on the underlying Yale Rotating Evolutionary Code (YREC; Demarque et al. 2008; Sills et al. 2000) whose interior models determine the evolving stellar structure.

2.1. *Initial Conditions*

One could, in principle, use the rotation distribution of T Tauri stars and model protostellar-disk interactions to obtain the initial conditions. Such an exercise is valuable when testing the origin of the distributions seen in young systems or when studying core-envelope decoupling. However, our focus is to investigate the impact of the observed spread of rotation rates on age estimates. We bypass model-induced uncertainties in the initial rotation distribution by adopting an empirical rotation distribution drawn from measurements of stellar rotation in a cluster.

Selecting the age to which models are initialized requires careful consideration. Stars do eventually forget their initial conditions as they spin down and converge to a common rotation-age sequence. Among clusters older than $\sim$ 500 Myr, the mass-rotation sequences for different clusters are consistent with being drawn from the same parent population (see Paper II). This commonality suggests that results obtained for a cluster older than 500 Myr may be extended to both other clusters in the same age regime and field stars. Using empirical distributions to set the initial conditions, however, does mean that the results are sensitive to the same biases and systematics present in the input cluster data. To mitigate this problem, we use a rich cluster with well understood biases, measures of completeness, and little field contamination, namely the open cluster M37 (NGC 2099). Hartman et al. (2008, 2009) performed a deep, 20 night survey with the MMT of M37, reaching down to $r \sim 23$ mag. They determined an age of 550±30 Myr (with overshooting), metallicity [M/H]=+0.045 ± 0.044, and distance modulus $(m-M)_V = 11.572 \pm 0.13$. reaching down to $r \sim 23$ mag. Searching for periodic variability using a multiharmonic AoV algorithm (Schwarzenberg-Czerny 1996) yielded a clean sample of 372 rotation period measurements. The sample is close to 100% complete to $r = 20$ mag (see Figure 9 in Hartman et al. 2009), in the sense of detecting stars with modulation above 0.01 mag, although the color-period diagram may be biased toward brighter stars. This means that an increasing fraction of cluster members have undetectable variations as mass declines. Hartman et al. estimate $\sim$ 20% contamination of the cluster sample by background field stars.

Hartman et al. obtained B, V, and I_C band photometry for this cluster. For a given set of isochrones, different colors resulted in consistent mass estimates in regimes where the isochrones were not double-valued. For this paper, we select $(V{-}I_C)_0$ to estimate mass because it has a large dynamic range and its relationship to mass remains monotonic for cool stars (see Figure 1). The $(V{-}I_C)$ photometry has been corrected for reddening $E(V{-}I_C)$=0.355 (Hartman et al. 2008) and compared to the corresponding 550 Myr, [Fe/H] = +0.045 YREC isochrone.

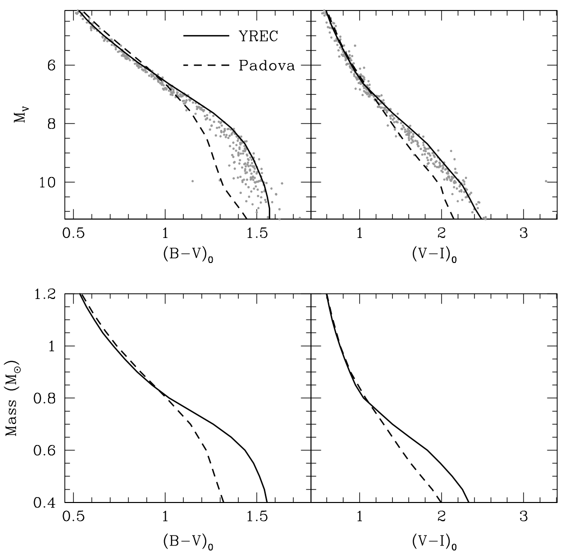

Fig. 1.— Color-magnitude diagrams (top) of M37 with YREC (solid) and Padova (dashed) [Fe/H]=+0.045 isochrones at 550 Myr overlaying the cluster main sequence (gray points). The corresponding color-mass relationships appear in the lower panels.

As demonstrated by Figure 1, the choice of isochrone induces larger shifts to the mass scale than the choice of color. The color-mass relationship for different isochrone systems agrees for bluer stars (masses > 0.75 $M_\odot$), but breaks down in the red. The YREC and Padova isochrones were selected because their differences produce the largest shift in the mass scale between any two widely-used isochrone systems. We note that the YREC isochrones better reproduce the morphology of the cluster main sequence compared to the Padova isochrones, so our error estimates will be conservative.

2.2. *Interiors*

We anchor our angular momentum study in theoretical models of stellar structure calculated using the YREC stellar interior models. We compute solar metallicity models (X=0.7190, Z=0.0165) with no diffusion. These provide a prior on a star's He abundance, radius, moment of inertia, convective overturn timescale (τ_{CZ}), and luminosity as a function of stellar mass and age.

The standard model of angular momentum loss described in §1.1 is only valid for stars in a particular mass range. Because stars above spectral type F8 show no obvious sign of a rotation-age relationship (Wolff et al. 1986), this sets an upper mass limit on where rotation-based ages are well motivated. The old open clusters have sparse data at the low mass end, and there is evidence for a departure from a Rossby scaled saturation threshold in that mass regime (Sills et al. 2000; see §2.4.1). Furthermore, quantities like τ_{CZ} become ill-defined for fully convective stars. We therefore restrict our calculations to the mass range of $0.4\ M_\odot \leq M \leq 1.2\ M_\odot$, sampled in equally spaced 0.05 $M_\odot$ intervals. Stars in M37 (used to define the initial rotation distribution, §2.1) are excluded if their mass lies outside of this restricted range where our angular momentum loss model is valid.

The empirically determined stellar masses and rotation rates from M37 set the initial conditions (§2.1). A prescription for angular momentum loss (§2.4) is used to simulate M37's rotational future. We calculate a star's angular momentum at each point in time on a logarithmically-spaced grid of ages. At fixed age, we perform a polynomial interpolation in logarithmic rotation period on a grid of models to the mass of the star.

We set the birth line by requiring that the deuterium abundance declines to a level of 0.1% below the initial value, resulting in a slight offset from the Sills et al. (2000) models. We stop our models if their age exceeds either a stars' lifetime on the main sequence or the age of the Galactic disk, assumed to be 10 Gyr. The main sequence turnoff is defined as the point when the core hydrogen abundance drops below $X_C = 10^{-3}$.

In accordance with standard mixing length theory, we define τ_{CZ} locally as $\tau_{CZ} = H_p/v_{conv}$ evaluated one pressure scale height above the base of the surface convection zone. In the YREC interior calculations, there is numerical jitter in τ_{CZ} at the $\lesssim 1\%$ level over a stars's main sequence lifetime. We therefore average τ_{CZ} over the five closest points in time to smooth over these numerical perturbations in the depth of the convection zone.

2.3. *Internal Angular Momentum Transport*

Core and envelope coupling timescales are short in comparison to the lifetime of G, K, and M dwarfs discussed here (e.g. Denissenkov et al. 2010; Spada et al. 2011). Because we are studying the rotation of field stars, assuming that the coupling timescale for angular momentum transport between the core and envelope is short (i.e. solid body rotation is enforced at all times) is a reasonable approximation for the majority of the age range of interest. This well motivated simplification has the added benefit of restricting the number of free parameters in the angular momentum loss law. The rotation rates in young systems are known to be influenced by core-envelope decoupling (e.g. Keppens et al. 1995; Krishnamurthi et al. 1998; Allain 1998; Irwin et al. 2007b; Collier Cameron et al. 2009; Denissenkov et al. 2010) and one purpose of our work is to infer the impact on global angular momentum evolution studies. We discuss tests of the coupling timescale by comparing results from clusters with ages close to and much older than the τ_c in Paper II. M37, the cluster used here to set initial conditions, falls into the latter category.

2.4. *Torque*

2.4.1. *Kawaler Wind Law*

To simulate stellar angular momentum loss, we adopt as our preferred model a modified Kawaler wind law (Chaboyer et al. 1995; Sills et al. 2000). Kawaler (1988) was able to recover the Skumanich (1972) law ($\omega \propto t^{-1/2}$) for his favored choice of the magnetic field geometry. This yields a wind law of the form $\mathrm{d}J/\mathrm{d}t = -K\omega^3 R^{1/2} M^{-1/2}$, where the normalizing constant K parametrizes our ignorance about winds and magnetic field generation in stars.

As initially conceived, this law does not account for magnetic saturation– a necessary element in the standard theory of angular momentum loss (§1.1). We follow Sills et al. (2000) in modifying the original Kawaler loss law to include a prescription for how the torque changes when a star's magnetic field strength saturates at a critical rotation rate ω_{crit}. Because the Reiners & Mohanty (2012) wind law (discussed in the next section §2.4.2) treats magnetic saturation differently, we supply a brief discussion of the empirical motivation and prior theoretical work that produced the functional form of the saturation threshold adopted here.

Observational studies of rotation and magnetic activity indicators support a Rossby-scaled magnetic saturation threshold. Both chromospheric Ca II H and K and coronal X-ray emission display a break in their relationship with Rossby number, where the Rossby number is $R_0 = \mathrm{P}_{\mathrm{rot}}/\tau_{CZ}$ (Noyes et al. 1984; Patten & Simon 1996). In fact, activity correlates more tightly with Rossby number than rotation period (Radick et al. 1987). Because measures of stellar activity serve as a proxy for magnetic field strength, which in turn powers the wind, the rate of angular momentum loss is also thought to plateau. Consequently, Krishnamurthi et al. (1997) proposed the addition of a Rossby scaled saturation threshold for stars more massive than 0.5 $\mathrm{M}_\odot$, resulting in the following modified Kawaler wind law:

$$\frac{dJ}{dt} = \begin{cases} -K\omega_{crit}^2\omega(\frac{R}{R_\odot})^{\frac{1}{2}}(\frac{M}{M_\odot})^{-\frac{1}{2}} & \text{for } \omega > \omega_{crit} \\ -K\omega^3(\frac{R}{R_\odot})^{\frac{1}{2}}(\frac{M}{M_\odot})^{-\frac{1}{2}} & \text{for } \omega \leq \omega_{crit} \end{cases} \quad (4)$$

where

$$\omega_{crit} = \omega_{crit,\odot}\frac{\tau_{CZ,\odot}}{\tau_{CZ}}. \quad (5)$$

From the solar mass YREC model, $\tau_{CZ,\odot} = 1.01 \times 10^6$ s. Because lower mass stars have deeper convection zones, τ_{CZ} contains the mass dependence in the saturation threshold.

X-ray measurements confine the saturation threshold ω_{crit} to the range 5 to 20 $\omega_\odot$ (Patten & Simon 1996). Sills et al. (2000) tested the Rossby scaling by comparing theoretical models to rotation distributions of IC 2602, IC 2391, α Per, the Pleiades, and Hyades. They found that the Krishnamurthi et al. (1997) scaling ($\omega_{crit,\odot} = 10\ \omega_\odot = 2.86 \times 10^{-5}\ \mathrm{s}^{-1}$ for solid body models) works for stars with masses between 0.6 $\mathrm{M}_\odot < M <$ 1.1 $\mathrm{M}_\odot$. However, the Rossby scaling breaks down for lower mass stars; Sills et al. argue that the saturation threshold drops more steeply than a Rossby scaling for stars with 0.1 $\mathrm{M}_\odot <$ M $<$ 0.5 $\mathrm{M}_\odot$. They then used the clusters to empirically measure the mass dependence of ω_{crit} for stars in this mass range. For solid body models, they find that $\omega_{crit,\odot}$ = 7, 6.2, 5.1, 3.6, and 1.7 $\omega_\odot$ at 0.5, 0.4, 0.3, 0.2, and 0.1 $\mathrm{M}_\odot$. We interpolate on the Sills et al. calibration for stars M $\leq$ 0.5 $\mathrm{M}_\odot$ and adopt the Krishnamurthi et al. calibration for M $>$ 0.5 $\mathrm{M}_\odot$.

Given this definition of ω_{crit}, Eq. 4 is calibrated such that a 1 $\mathrm{M}_\odot$ star achieves the solar rotation rate $\omega_\odot = 2.86 \times 10^{-6}$ rad s^{-1} (the Sun's equatorial rotation period is $\mathrm{P}_\odot$ = 25.4 days) at the solar age of 4.5 Gyr starting with an initial period of 10 days and no disk locking. This results in $K_\odot = 3.15 \times 10^{47}$ g cm^2 s. The choice of initial rotation period is plausible; it is similar to the average T Tauri rotation period of 9.45 days measured by Choi & Herbst (1996) in the ONC. However, the predicted rotation period at the age of the Sun, and therefore the value of the normalization constant, is highly insensitive to the choice of initial rotation period. This is a characteristic feature of angular momentum laws of with a strong dependence on rotation rate, namely, that once stars enter the unsaturated regime ($\omega \leq \omega_{\mathrm{crit}}$), they rapidly forget their initial conditions. For example, if

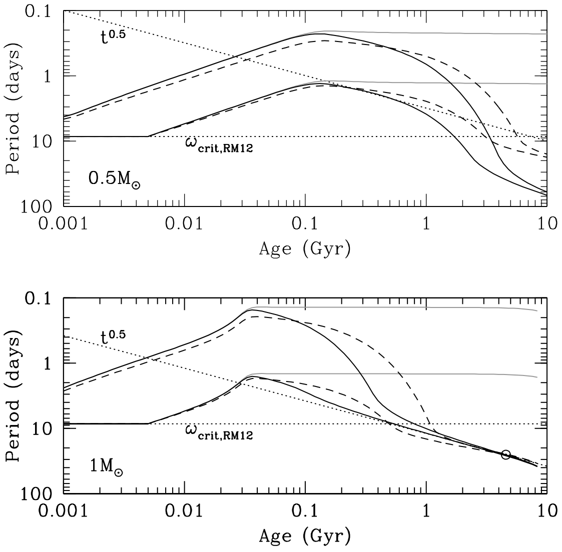

FIG. 2.— Rotation period evolution according to the modified Kawaler (Eq. 4; solid) and Reiners & Mohanty (Eq. 6; dashed) braking laws for a 0.5 $\mathrm{M}_{\odot}$ (top) and 1 $\mathrm{M}_{\odot}$ (bottom) star. All models assume an initial rotation period of 8.5 days. Evolutionary tracks are shown for scenarios with 0 and 5 Myr of disk-locking. The Reiners & Mohanty law has been re-calibrated such that it reproduces the Sun with the YREC interior models. The diagonal dotted line gives the solar calibrated Skumanich $P \sim t^{0.5}$ relation, calibrated to the Kawaler law at 550 Myr with 5 Myr disk-locking (top) and to the Sun (bottom). The horizontal dotted line shows the mass- and time-independent saturation threshold adopted by Reiners & Mohanty (2012). Grey solid lines show the case of no braking for comparison.

we instead calibrated the solar rotation rate with an initial period of 10 days and a 5 Myr disk locking time, this would result in a slightly different normalization constant $K_{\odot} = 2.97 \times 10^{47}$ g cm^2 s.

2.4.2. *Reiners & Mohanty Wind Law*

Reiners & Mohanty (2012) present a new braking law that pivots on two major deviations from the modified Kawaler law. First, Reiners & Mohanty argue that rotation is related to the magnetic field strength ($B_0 \propto \omega^a$) rather than the surface magnetic flux ($B_0 R^2 \propto \omega^a$) as assumed in Kawaler (1988). This factor of R^2 difference has powerful ramifications when propagated to the angular momentum loss law. Second, Reiners & Mohanty assume that the saturation threshold ω_{crit} does not depend on mass. This differs from the Rossby-scaled saturation threshold used in §2.4.1; in this new law, the saturation threshold is insensitive to structural differences in stellar interiors. The reader should refer to Reiners & Mohanty (2012) to see the specifics of their derivation, but the resulting angular momentum loss law (their Eq. 5) is reproduced below:

$$\frac{dJ}{dt} = \begin{cases} -\,\mathcal{C}\;\omega\left(\frac{R^{16}}{M^2}\right)^{1/3} & \text{for } \omega \geq \omega_{\mathrm{crit}} \\ -\,\mathcal{C}\left(\frac{\omega}{\omega_{\mathrm{crit}}}\right)^4 \omega\left(\frac{R^{16}}{M^2}\right)^{1/3} & \text{for } \omega < \omega_{\mathrm{crit}} \end{cases} \tag{6}$$

where $\mathcal{C}$ is a constant relating to the magnetic field strength and rate of mass loss, R is stellar radius and M is stellar mass in cgs units. It is important to note that Reiners & Mohanty use the saturation threshold in the opposite sense of the modified Kawaler law. In the saturated regime ($\omega \geq \omega_{\mathrm{crit}}$), the rate of spin down is set by a maximum magnetic field strength ($\mathrm{B}_{\mathrm{crit}}$) for all stars. The saturation threshold ω_{crit} only affects the torque in the *unsaturated* regime ($\omega < \omega_{\mathrm{crit}}$). This means that changing the saturation threshold affects the late-time behavior of stars under the Reiners & Mohanty (2012) prescription. This is not true for a modified Kawaler law, where the effect of ω_{crit} is only felt in the saturated regime and erased as stars forget their initial conditions.

To calibrate this wind law, Reiners & Mohanty match the solar rotation rate at the solar age, starting with an initial rotation rate of 8.5 days. The presence of a disk is assumed to hold the rotation rate constant for 5 Myr. This yields their best fit combination of parameters $[\omega_{\mathrm{crit}},\ \mathcal{C}] = [8.56\times10^{-6}\ \mathrm{s}^{-1},\ 2.66\times10^{3}\ (\mathrm{g}^5/\mathrm{cm}^{10}\mathrm{s}^3)^{1/3}]$. We recalibrate the constant $\mathcal{C}$ to reproduce the Sun with our models and a 5 Myr disk-locking lifetime, finding a different value of $\mathcal{C} = 3.16\times10^{2}\ (\mathrm{g}^5/\mathrm{cm}^{10}\mathrm{s}^3)^{1/3}$.

Figure 2 compares angular momentum evolution under both a modified Kawaler and a Reiners & Mohanty wind law with and without a disk. The largest differences appear among low mass stars. As discussed in §2.4.1, Sills et al. (2000) find that the Rossby scaling is inadequate for stars $< 0.6\ \mathrm{M}_{\odot}$. The Reiners & Mohanty law naturally preserves rapid rotation of low mass stars. For solar mass stars, the Kawaler wind law asymptotes to the Skumanich relationship, becoming nearly indistinguishable by 500 Myr in the disk-locked case. In contrast, the Reiners & Mohanty wind law predicts a slower spin down than Kawaler does for the first few Myr, followed by an interval of rapid angular momentum loss between $\sim 200 - 700$ Myr, before leveling off and approaching a rate slightly shallower than Skumanich later in life.

3. RESULTS

Because the timescale for rotational evolution is faster than that of nuclear burning for low mass stars, rotation represents a promising tool for measuring stellar ages. Here we explore the potential of using rotation as a clock for field stars. Having initialized our clock in §2, we now test how it runs compared to other timepieces. Section 3.1 compares our models' median rotation-mass-age relationship with published gyrochonology relations. These theoretical predictions are then evaluated by their agreement with the independently-measured age of two binary star systems, and also with slowly rotating field stars. Such empirical guidance is necessary for discriminating between different theoretical prescriptions.

Until now, clockmakers have focused on how well rotation-based clocks keep time, but largely ignored the precision of those measurements. In §3.2, we investigate many sources of error that can affect rotation-based ages. The dominant source of uncertainty for low mass stars proves to be the intrinsic scatter in the initial rotation distribution. Because these stars require many Gyr to converge to a unique rotation-mass-age relationship, this induces large uncertainties in rotation-based ages. Among old stars, the range of surface rotation rates observable due to latitudinal differential rotation limits the precision. Systematic uncertainties due to modeling choices are also discussed.

Stars, like mechanical clocks, wind down over time.

More slowly spinning stars tend to be less magnetically active and their amplitude of variability declines (Skumanich 1972). Past a certain age, the variability will become too small to be detectable from the ground. In §3.3, we determine that this technique of measuring rotation-based ages is feasible for stars as old as 1–2 Gyr using groundbased surveys, but space-based instruments are required to see photometric modulation in older populations. Comparison of our predictions with rotation periods detected by current groundbased surveys suggests that our predictions may be too conservative and that such studies may probe even older populations.

3.1. *Median Rotation-Mass-Age Relationships*

Because currently-studied open clusters only provide guidance for stellar angular momentum evolution < 1 Gyr, we utilize the angular momentum loss models described in §2 to forecast rotational behavior over the lifetime of the Galactic disk. Section 3.1.1 characterizes how both the median and shape of the rotation distribution evolve over time for two angular momentum loss models. The rate at which stars converge to a unique rotation-mass-age sequence sets the timescale for when rotation becomes a useful clock. We compare the median rotation-mass-age trends for these models with published gyrochronology relationships in §3.1.2. Because some of the gyrochronology relationships fail to reproduce the median trend seen in the M37 cluster data, we question the calibration of these relationships.

Although observational constraints on the rotation-mass-age relationship are rare at late times, two binary star systems, 61 Cyg and α Cen, possess independent age measurements. We therefore test the rotation-based age predictions from our models and published gyrochronology relationships against these binaries in §3.1.3. In the case of these old binary stars, latitudinal surface differential rotation induces ~ 2 Gyr uncertainties in rotation-based age estimates. We also consider the implications for these angular momentum evolution models of long rotation periods observed for old field stars.

3.1.1. *Time Evolution of M37's Rotation Distribution*

Young clusters display a large spread in stellar rotation rates across all masses. This wide range converges as stars age, but the timescale for this process can be long, especially in lower mass dwarfs. We begin by modeling the time evolution of M37's rotation distribution and investigating how long it takes for rotation rates to converge. The timescale for convergence is important because the median rotation-mass-age relationship only becomes a good chronometer after stars have forgotten their initial conditions.

The description in §2 provides the theoretical framework necessary to predict the rotation of a star at any future time, given its mass and initial period. We use solid body models to evolve M37's rotation distribution from 550 Myr forward in time. We explore two different prescriptions for the torque, starting with a modified Kawaler wind law (§2.4.1). Figure 3 shows M37's initial rotation distribution at 550 Myr and also how that distribution would evolve under the influence of a modified Kawaler wind law. For visual clarity, we show the projected distribution at representative ages 1, 2, 5, and 10

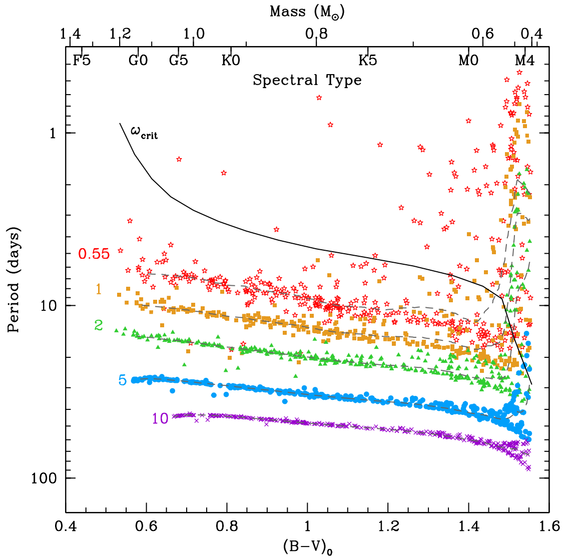

FIG. 3.— M37's color-period distribution (Hartman et al. 2009) evolved forward in time from 0.55 Gyr (red stars) to 1 Gyr (gold squares), 2 Gyr (green triangles), 5 Gyr (blue circles), and 10 Gyr (purple crosses). The corresponding ages (in Gyr) are indicated to the left of the mass-rotation sequence. These synthetic rotation distributions are created by evolving the M37 rotation distribution forward in time with the modified Kawaler spin down model described in §2.4.1. The black curve shows the critical rotation rate (ω_{crit} at 550 Myr) above which stars fall in the saturated regime. The dashed curves show the median rotation period at each age. The associate mass and spectral type are given along the top axis. Masses are taken from a 1 Gyr, [Fe/H]$_{\rm M37}$=+0.045 YREC isochrone. Convergence occurs later for redder (lower mass) stars.

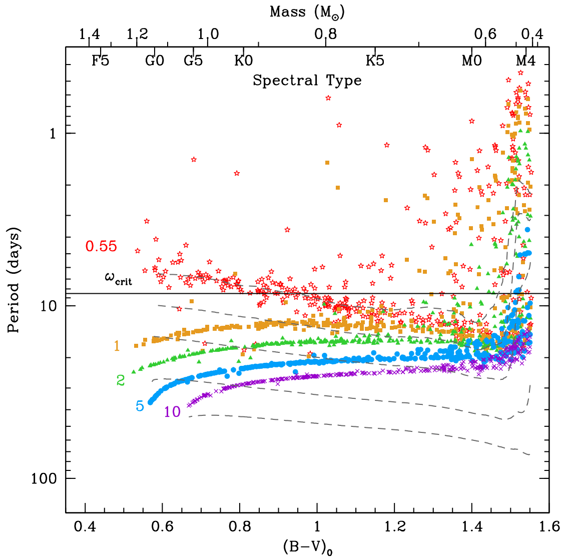

FIG. 4.— In analogy to Figure 3, M37's color-period distribution (Hartman et al. 2009) evolved forward in time from 0.55 Gyr (red stars) to 10 Gyr (purple crosses) according to the Reiners & Mohanty (2012) braking law described in §2.4.2. The corresponding ages (in Gyr) are indicated to the left of the mass-rotation sequence. The black line shows the constant critical rotation rate (ω_{crit}=8.56×10^{-6} s^{-1}). The dashed lines indicate the corresponding medians from the Kawaler wind law (Figure 3) for comparison. The associate mass and spectral type are given along the top axis. Masses are taken from a 1 Gyr, [Fe/H]$_{\rm M37}$=+0.045 YREC isochrone.

Gyr. Even in the initial cluster distribution at 550 Myr, bluer stars have begun to form a mass-rotation sequence. Because of the rotation-dependent rate of angular momentum loss (Eq. 4), this sequence becomes tighter over time and redder stars converge to join it.

The vertical displacement of the coeval distributions reflects the fact that stars spin more slowly with time. The reddest stars in the cluster exhibit a large dispersion in rotation rate at young ages, but this range also shrinks over time. Nonetheless, a star with spectral type M4 and a rotation period of 20 days easily falls within the overlapping range of the 0.55, 1, and 2 Gyr distributions, but could also be among the most rapidly rotating members of even older populations. This inherent ambiguity represents a fundamental uncertainty in rotation-based ages and will be discussed in depth in §3.2.1.

The median mass-rotation curves at a series of ages may be inverted to provide rotation-based ages when the scatter about the median is small. However, we note that rotation rates still encode age information, even in situations when a star's mass and rotation rate does not correspond to a unique age. If the form of the distribution was known, and the rate of change calibrated, one could in principle obtain statistical information about ages even when the rotation-age solution is not unique. A probability distribution for the age of a star with a given mass and rotation period could be constructed by weighting these iso-age rotation distributions by the rate of star formation and the rate of angular momentum evolution. Given the uncertainties associated with the rates necessary to this calculation, we instead focus on the median rotation-mass-age relationship here and use the range of rotation to quantify the uncertainty in rotation based ages in §3.2.

For comparison, we also explore the the effect of using a different angular momentum loss law. We begin with the same M37 rotation distribution at 550 Myr, but this time we use the Reiners & Mohanty wind law (§2.4.2) to model angular momentum evolution. Figure 4 shows how the shape of the M37 distribution changes under the Reiners & Mohanty wind law compared to the modified Kawaler wind law (Figure 3). Conspicuously, the slope of the mass-rotation relationship appears to flip between 550 Myr and 1 Gyr. This arises from a combination of negligible spin down for low mass stars and an interval of rapid spin down for solar-type stars as noted in Figure 2. After 1 Gyr, the rate of angular momentum loss predicted by the Reiners & Mohanty law slows for stars of all masses, maintaining the inverted slope of the mass-rotation sequence established earlier.

The dashed lines in Figure 4 reproduce the median mass-rotation sequences from the Kawaler law. The difference between the Reiners & Mohanty and Kawaler sequences is striking. In addition to having slopes of a different sign, the Reiners & Mohanty law produces a smaller torque than the Kawaler law. To wit, the Kawaler law spins M < 0.9 M$_\odot$ stars down to rotation periods slower than they achieve in 10 Gyr with the Reiners & Mohanty law– in half the time! Because of the compressed dynamic range of rotation rates in the Reiners & Mohanty law compared to Kawaler, the overlap between iso-age populations is more extreme for low mass stars. The reddest stars have such weak predicted spin down with a Reiners & Mohanty law that the 550 Myr and 10 Gyr distributions overlap. In this regime where spin down failed to separate iso-age populations, the overlap creates ambiguous rotation-based age predictions covering a wide range. To extract more information, one must rely on statistical ages.

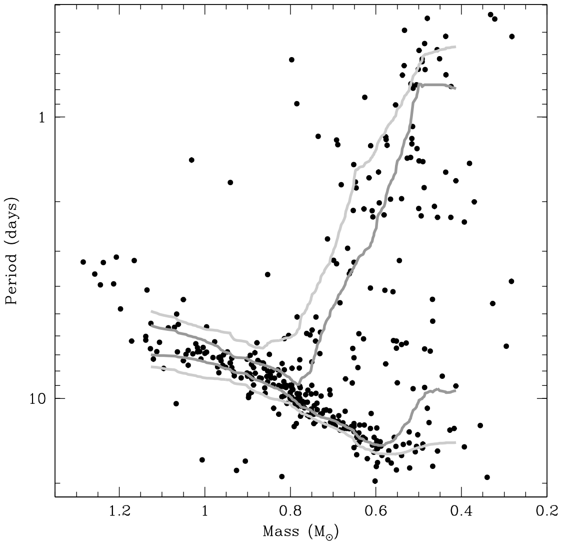

Fig. 5.— Mass-period distribution for M37 sample Hartman et al. (2009). The dark gray band marks the smoothed 25th and 75th period percentiles. The light gray band depicts the smoothed 10th and 90th period percentiles We generally adopt the interquartile region as the proxy for width of the rotation distribution, although the impact of using the inner 80% region instead is discussed in §3.2.3.

Now that we have two predictions for how M37's rotation distribution evolves in time, we need to characterize their median trend and range. To quantify the width of the rotation distribution, we adopt the interquartile range in period. We calculate the 25th and 75th percentile in a moving window of 25 stars per mass bin and perform a smoothed boxcar average with a width of 50 stars to flatten out any star-to-star jitter in the calculated percentiles. The middle 50% of stars in the observed M37 cluster mass-rotation distribution lie within the interquartile band shown in Figure 5 and we use this to characterize the spread between fast and slow rotators throughout most of the paper. The median is calculated with the same bins and smoothing as for the interquartile region.

For comparison, we also consider the 10th and 90th percentile rotation periods because they set much broader bounds than the interquartile region, but are not overly sensitive to outliers in the rotation distribution. We calculate the 10th and 90th percentile in a moving window of 25 stars per mass bin and perform a smoothed boxcar average with a width of 80 stars. The middle 80% of stars in the observed M37 cluster mass-rotation distribution fall within the light gray band shown in Figures 5. The effect of choosing this alternative metric for the width of the rotation distribution is discussed in §3.2.3.

The percentile ranges in Figure 5 clearly illustrate that higher mass stars have converged to a narrow mass-rotation sequence by the age of M37. Toward lower masses, the distribution rapidly fans out to span over a decade in period. This sharp transition may be used to define the point of convergence for which more massive stars have forgotten their initial rotation rates and converged to a tight sequence. We choose to define the point of convergence as the place where the width of the distribution is comparable (within a factor of 2) to the measured period uncertainties. As we shall see later, surface differential rotation limits the precision of rotation period measurements. In §3.2.2, we adopt a minimum uncertainty of 10% to reflect the range of surface rotation rates at different latitudes. Thus, we define our criterion for convergence to be when the interquartile region is smaller than 20% of the median rotation period. This also qualitatively reproduces the by-eye location of the abrupt widening of the distribution.

By this metric, a converged sequence is established down to $(B–V)_0$ =1.08 (M=0.78 $M_\odot$) at the starting age of 0.55 Gyr. For the Kawaler wind law, the mass-rotation sequence is converged to $(B–V)_0$ =1.17 (0.74 $M_\odot$) by 1 Gyr, to $(B–V)_0$ =1.41 (0.62 $M_\odot$) by 2 Gyr, to $(B–V)_0$ =1.50 (0.52 $M_\odot$) by 5 Gyr, and to $(B–V)_0$ =1.54 (0.46 $M_\odot$) by 10 Gyr. By the same rule, the Reiners & Mohanty distributions are converged to $(B–V)_0$ =1.19 (0.73 $M_\odot$) by 1 Gyr, to $(B–V)_0$ =1.33 (0.67 $M_\odot$) by 2 Gyr, to $(B–V)_0$ =1.46 (0.58 $M_\odot$) by 5 Gyr, and to $(B–V)_0$ =1.54 (0.45 $M_\odot$) by 10 Gyr. It is interesting that the location of the point of convergence is robust to within 0.06 $M_\odot$ even though these two models treat the saturation threshold differently. These points define the red boarder of the regime where the distribution of rotation rates has tightened enough that the median rotation-mass-age relationship can provide good constraints on age under one of these wind laws.

3.1.2. *Comparison to Published Gyrochronology Relationships*

In the previous section, we quantified both the median rotation-mass-age relationship and range of rotation rates for two different angular momentum loss laws. Here, we reconcile those trends with the literature. Published gyrochonology relationships ignore rapidly rotating stars and focus on describing the shape and time-evolution of the sequence of slowly-rotating stars in open cluster samples (for further discussion, see §1.2 and references therein). For the purposes of comparison, we concentrate on the median trend and postpone further discussion of the width of the rotation distribution until §3.2.

Figure 6 shows the median mass-rotation relationship obtained by evolving the M37 rotation distribution forward with both a modified Kawaler and Reiners & Mohanty wind law (from §3.1.1). It also features the predictions of three gyrochronology relations (Barnes 2007; Mamajek & Hillenbrand 2008; Meibom et al. 2009), with the functional form of Eq. 1 and parameters specified by Table 1.

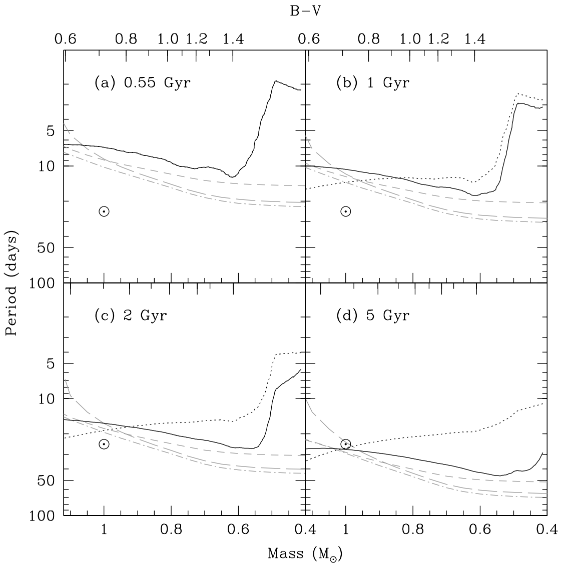

FIG. 6.— Median mass-period relationship for a Kawaler (black solid) and Reiners & Mohanty (black dotted) wind law at fixed age ranging from 0.55 Gyr (a) to 5 Gyr (d). Isochrones for three gyrochronology relations (Barnes 2007, dash-dot; Mamajek & Hillenbrand 2008, short dash; and Meibom et al. 2009, long dash) are shown in gray for comparison. For reference, the Sun is shown at its current equatorial rotation period in all panels. The color-mass conversion used YREC isochrones of the respective age and [Fe/H]=+0.045.

The medians show a steep upturn at low mass that is not present in the gyrochronology curves. This underscores a fundamental difference: the median is a measure of the entire distribution, while published gyrochronology relationships are calibrated only to the slow rotators. A comparison between these two is fair in the converged regime because there the entire rotation distribution has collapsed to the narrow, slowly-rotating band fit by gyrochronology relationships. Figure 6 may be interpreted by assuming everything to the left of the upturn in the median trend falls in the converged regime (see §3.1.1 for a more formal definition of the point of convergence.)

Although open clusters provide information about rotation in the young stars, the Sun is the only point used to calibrate angular momentum evolution models at ages older than 1 Gyr. Given its significance, we first check how well these models reproduce the Sun. For a visualization, panel (d) comes the closest in age to the Sun at 5 Gyr. By definition, the modified Kawaler and Reiners & Mohanty (2012) medians reproduce the Sun at the solar age. Two of the three gyrochronology relations also match the Sun's equatorial rotation rate within ±1 day. The third, Meibom et al. (2009), predicts a rotation period ~ 20 days for the Sun because they did not use it as a calibration point. Instead, Meibom et al. retained the time-dependence from Barnes (2007) while changing the color-rotation function $f(B-V)$ to fit the open cluster M35. Nonetheless, the gyrochronology relations best agree with our median rotation-mass-age relations near solar color.

For stars redder than the Sun, all three gyrochronology relations spin stars down too quickly, resulting in predicted rotation periods that are too long by a factor of $1.5-2$ relative to a modified Kawaler spin down model. These published relations display zero-point differences relative not only to theory (panels b-d), but also to the observed rotation distribution of M37 (panel a). We note that the coupling timescale is shorter than the age of M37 (Denissenkov et al. 2010), so this cluster's rotation distribution should reflect the true angular momentum content of its stars. Gyrochronology relationships may predict rotation rates that are too slow because they are calibrated to younger clusters with stars whose core and envelope have not yet re-coupled. If the surface rotation rate masks a reserve of angular momentum in the core, gyrochronology relations would propagate forward the superficial rotation rate and predict artificially slow rotation at late times.

Mamajek & Hillenbrand (2008) noticed that the Barnes (2007) relation predicted rotation periods 50% longer than those found in the Hyades. To address this, Mamajek & Hillenbrand carefully selected only stars that clearly lie on the converged sequence to include in their fit to the mass-rotation function $f(B-V)$. As a result, the Mamajek & Hillenbrand isochrones reproduce the shape of the mass-rotation sequence better than other gyrochronology prescriptions. Differences between the shape of the gyrochronology curves and the median of the M37 data in panel (a) arise strictly from problems in the calibration of gyrochronology relations in young and intermediate age clusters. However, additional time-dependent differences can also arise because our angular momentum models evolve in time and the gyrochronology relations remain self-similar. Two effects in particular can impact the rotation distribution and therefore its median: evolutionary changes to stellar structure and magnetic saturation. The former is most important for the rapidly evolving, relatively high mass stars. The prescriptions for $\dot{J}$ also depend on the mass and radius. This structural dependence is much more signficant for the Reiners & Mohanty law than for the modified Kawaler law. Magnetic saturation is important for both loss laws. In the case of the modified Kawaler law, only low mass stars rotate faster than the saturation threshold at the age of M37 because of the Rossby-scaling (see Figure 3 and Eq. 5). In contrast, the saturation threshold is constant in the Reiners & Mohanty law and affects stars of all masses because of the way it cuts through M37's rotation distribution (Figure 4). Together these two effects can have a mild (modified Kawaler) to significant (Reiners & Mohanty) time-dependent impact on the median rotation-mass-age relationship.

3.1.3. *Tests in Old Field Stars: The Importance of Differential Rotation*

Older than 1 Gyr, the rotation-mass-age relationships described in §3.1.2 are constrained only by sparse data, primarily calibrated on the Sun. We are fortunate to possess rotation period and age measurements for two wide binaries. These old field stars can test whether the solar-calibrated rotation-mass-age relationship holds for stars with a mass and age different than the Sun.

Because stars lack a uniform surface rotation rate, any rotation period measurement of a star will be drawn from some distribution of surface rotation periods. If you measure a rotation period using a near-polar starspot, it will yield a different rotation period relative to an equatorial starspot because of latitudinal differential rotation (e.g. Barnes et al. 2005; Reiners 2006.) The Sun exhibits differential rotation, with a rotation period of 25.4 days at the equator and 36 days around its poles (e.g. Schou et al. 1998; Beck 2000 and references therein). Disk integrated Ca II K-line measurements yield a range of rotation rates from 24.5 (lower than the true equatorial rotation rate due to measurement error) to 28.5 days, with a mean of 26.09 days (Donahue et al. 1996). Below, we investigate the data available for the two binary star systems: 61 Cyg and α Cen.

61 Cyg

Donahue et al. (1996) present the measurement of a range of rotations for 36 stars with five or more seasons of detectable periodic modulation in the Ca H and K emission from the Mount Wilson survey. Among these, the K5V+K7V binary 61 Cyg (HD201091 and HD201092) is of particular interest because it is physically well characterized. Donahue et al. report mean rotation periods $\langle P\rangle_A = 35.37$ days and $\langle P\rangle_B = 37.84$ days with periods ranging from 26.82–45.25 days for 61 Cyg A and 31.78–46.57 days for B. The surface metallicity is spectroscopically measured as $[\mathrm{Fe/H}]_A = -0.20 \pm 0.10$ and $[\mathrm{Fe/H}]_B = -0.27 \pm 0.19$ (Luck & Heiter 2005). The high-accuracy parallax information from van Altena et al. (1995) and the *Hipparcos* catalog (Perryman & ESA 1997) tightly constrains the luminosity to $\mathrm{L}_A = 0.153 \pm 0.010\ \mathrm{L}_\odot$ and $\mathrm{L}_B = 0.085 \pm 0.007\ \mathrm{L}_\odot$. Combining the parallax with interferometric radius measurements, Kervella et al. (2008) found $\mathrm{R}_A = 0.665 \pm 0.005\ \mathrm{R}_\odot$ and $\mathrm{R}_B = 0.595 \pm 0.008\ \mathrm{R}_\odot$. Two measurements of the mass exist: 0.67 and 0.59 $\mathrm{M}_\odot$ (Walker et al. 1995) and 0.74 and 0.46 $\mathrm{M}_\odot$ (Gorshanov et al. 2006) for 61 Cyg A and B, respectively. Kervella et al. (2008) used observational constraints to construct CESAM2k evolutionary models (Morel 1997) and derive masses $\mathrm{M}_A = 0.690$ and $\mathrm{M}_B = 0.605\ \mathrm{M}_\odot$ and an age of 6 ± 1 Gyr.

We adopt the Kervella et al. masses and re-derive the age with YREC models. We evolved models using the input physics described in van Saders & Pinsonneault (2012), adopting a solar calibrated mixing length of $\alpha = 1.926$ and $\mathrm{Y} = 0.265$. The initial metallicity was chosen to yield a surface [Fe/H] of -0.20 at an age of 6 Gyr. We matched the radius within the errors at ages of 5.7 ± 1.2 and 7.5 ± 2.5 Gyr for 61 Cyg A and B respectively. This yields an age of 6 ± 1.4 Gyr for the system as a whole, to be compared with the age of 6 ± 1 Gyr derived using the CESAM code (Kervella et al. 2008) with the same masses and helium, but different choices of metallicity and mixing length. However, we believe that this underestimates the age error, as an additional 1 Gyr systematic results from varying the metallicity with the observational error of 0.1 dex. We therefore adopt 6.0 ± 1.7 Gyr as our age for the system.

α Cen

The proximity of α Cen allows the precise determination of the fundamental parameters for its component G2V+K1V stars. We adopted the same physical parameters as Eggenberger et al. (2004). These include precise parallaxes (Söderhjelm 1999), masses (Pourbaix et al. 2002), radii (Kervella et al. 2003), and temperatures (Neuforge-Verheecke & Magain 1997; Morel et al. 2000). Detections of p-mode oscillations in both α Cen A and B provide seismic constraints on the central helium abundance and age of the star (Bouchy & Carrier 2002; Carrier & Bourban 2003). Combining all of these non-seismic and seismic constraints, Miglio & Montalbán (2005) found an age of 6.8 ± 0.5 Gyr for α Cen. As described above, we created a YREC model for stars of mass M_A=1.105, M_B=0.934 and $\mathrm{Z} = 0.0302$, $\mathrm{Y} = 0.275$ (Eggenberger et al. 2004).

Because α Cen is not observable from the northern hemisphere, long-term monitoring of rotation rates from

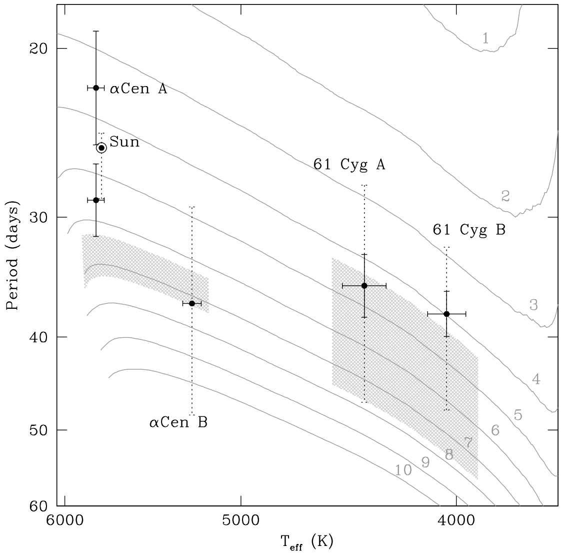

Fig. 7.— Location of the Sun and wide binaries α Cen and 61 Cyg in the effective temperature-rotation period plane. The Mount Wilson survey measured the range of observed rotation periods over many seasons due to surface differential rotation (dashed), mean rotation rate (point), and error in the mean (solid) for the Sun and 61 Cyg (Donahue et al. 1996). Because α Cen lacks such detailed rotation measurements, we show the two measurements available for α Cen A and assume that α Cen B displays a range in rotation rates similar to 61 Cyg A, which has a similar rotation period. The gray contours represent the median temperature-period relation for stars with age 1–10 Gyr, assuming a modified Kawaler wind law and YREC isochrones. The hatched regions illustrate the region consistent with the isochrone ages for the two binaries.

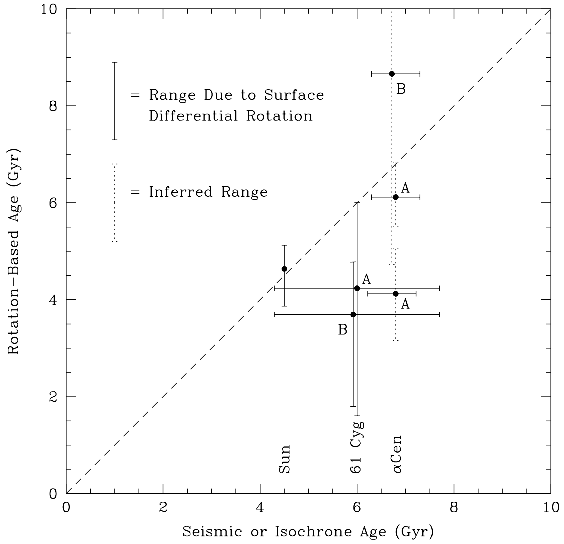

Fig. 8.— Comparison of rotation-based age with isochrone age for the Sun and wide binaries α Cen and 61 Cyg. Rotation based ages calculated according to the median temperature-rotation relationship. As in Figure 7, the observed range of rotation rates are measured for the Sun and 61 Cyg. Since α Cen B has a single rotation period measurement, its range is assumed to be of comparable size to 61 Cyg A. Two individuals measurements of rotation period are shown for α Cen A, which together can be taken to set a minimum on its observed range of rotation rates. For clarity, the central age values of 61 Cyg B and α Cen B have been offset slightly from their true isochrone age.

the Mount Wilson survey are not available. We refer to Mamajek & Hillenbrand (2008), which cites two measurements of rotation period for α Cen A: 22 ± 3 days (Guinan 2008, private communication) and 28.8 ± 2.5 days (Hallam et al. 1991). The rotation period of α Cen B is measured as 36.9 ± 0.5 days (Jay et al. 1997) from the 1995 IUE data set (a more recent analysis of the same data yields a nearly identical result 36.2 ± 1.4 days, DeWarf et al. 2010). Because α Cen B has only one independent measurement of its rotation period, we assume that its surface differential rotation produces a range of rotation rates as large as 61 Cyg A. This is a reasonable assumption since α Cen B and 61 Cyg A possess similar rotation periods and Donahue et al. (1996) found a strong correlation between mean rotation period and the range of observed rotation rates.

Surface Differential Rotation in Binaries

Although individual rotation periods may be measured precisely, they are drawn from a range of rotation periods corresponding to the latitude of the active region on the stellar surface. The range of rotation periods observed for the Sun and 61 Cyg and inferred for α Cen are shown in Figure 7. These ranges are compared with the median rotation curves evolved forward in time from the M37 rotation distribution assuming a modified Kawaler wind law.

Because binaries form coevally, the rotation rates of individual components should lie along the same rotational isochrone. Furthermore, the shaded regions indicate the range of rotation periods consistent with the seismic age of α Cen A and isochrone age of 61 Cyg. The measured rotation periods for 61 Cyg A cover a broad range of ages from approximately 3–9 Gyr. The hatched region corresponds to the range of rotation periods expected for a star with age 6.0 ± 1.7 Gyr. Both components of 61 Cyg are consistent with the isochrone age and with each other.

For α Cen, the tightly constrained seismic age is consistent with the B component and the longer period measurement (Hallam et al. 1991) of A's rotation period. The short period measurement of α Cen A rotation compared to the isochrone age demonstrates that any single measurement can have a ~ 2 Gyr error in its rotation-based age due to surface differential rotation.

To better quantify the range in rotation-based ages due to a range in observed rotation rates, we model the angular momentum evolution of these stars using a modified Kawaler wind law and the customized stellar evolutionary tracks described above. The initial rotation period is set to M37's median rotation period at the corresponding temperature and is evolved forward from 550 Myr. We use temperature as the coordinate to compare the near-solar metallicity M37 rotation distribution with the binaries, which have different metallicities and therefore different mass-color relationships, because the convective properties that govern angular momentum evolution are primarily set by T$_{\mathrm{eff}}$. We interpolate on this track to determine the rotation-based age corresponding to range of observed rotation rates. The results are compared with the seismic age of α Cen or the isochrone age of 61 Cyg as shown in Figure 8.

Because these ages were computed with customized tracks, they will differ from the ages read off the near solar-metallicity M37 contours shown in Figure 7. In particular, this drives rotation-based ages for the slightly metal-poor and lower mass 61 Cyg into worse (1σ–2σ) agreement with its isochrone age, which hints at a possible metallicity dependence to the angular momentum loss law. Because the only point of calibration for loss laws at ages $\gtrsim 1$ Gyr is the Sun, it is conceivable that stars of a different metallicity or mass would behave differently beyond the regime tested by clusters. The Kepler mission will create a sample of field stars with asteroseismic ages capable of calibrating the metallicity dependence of the rotation-mass-age relationship.

We also perform an identical calculation using the Reiners & Mohanty (2012) wind law and the customized tracks. The Reiners & Mohanty models do not spin down to periods longer than 30 days for α Cen B and 61 Cyg A and B within 10 Gyr. This model then fails to provide a reasonable rotation-based age for these binary components. Reiners & Mohanty (2012) note a related problem for field M stars, which are below the mass range considered here. However, even for K dwarfs slowly rotating stars exist with well measured ages younger than 10 Gyr. This indicates that the late time behavior of the Reiners & Mohanty law as published does not appropriately capture true stellar behavior even for higher mass dwarfs. Further discussion of the Reiners & Mohanty (2012) law appears in §3.2.6.

If the Reiners & Mohanty rotation-based ages are too old, some published gyrochronology relationships produce ages that are too young. We compare the two solar-calibrated published gyrochronology relationships against these binaries and determine that the Mamajek & Hillenbrand (2008) relation is consistent while the Barnes (2007) formalism is not. Mamajek & Hillenbrand (2008) already performed this comparison, finding an age (in years) of $\log t_A = 9.57$ and $\log t_B = 9.53$ of 61 Cyg's components using their mean rotation period, which average to $\langle \log t_{61\mathrm{Cyg}} \rangle = 9.55$. Although this mean age (3.52 Gyr) is too young compared with the isochrone age of 61 Cyg (6.0 ± 1.7 Gyr), including the full range of rotation observed in 61 Cyg broadens the range of rotation-based ages to $2.25 < t_A < 5.66$ Gyr and $2.48 < t_B < 4.87$ Gyr. Similarly, for α Cen, Mamajek & Hillenbrand report $\langle \log t_{\alpha\mathrm{Cen}} \rangle = 9.70$ (5.01 Gyr), which is inconsistent with the seismic age (6.8 ± 0.5 Gyr) at the 3.6σ level if the gyroage is treated as exact. With the inferred range of rotation periods, the tension between the seismic age and the Mamajek & Hillenbrand age ranges ($3.64 < t_A < 5.86$ Gyr and $4.77 < t_B < 5.47$ Gyr) decreases to the $\sim 2\sigma$ level. Thus, the mean Mamajek & Hillenbrand trend is consistent with these binaries, but their estimated errors are too small. Mamajek & Hillenbrand take the difference in predicted rotation-based ages of these coeval binary components as the error. They find an uncertainty of ±11% in gyrochronology predictions, similar to the total error of 15% from Barnes (2007). These error estimates ignore systematic sources of uncertainty in rotation-based ages, including surface differential rotation, which we will discuss in §3.2.

We next consider the Barnes (2007) relationship. For conciseness, we write the age corresponding to the mean and range due to surface differential rotation in a condensed format. For 61 Cyg, the Barnes relation yields ages of $t_A = 2.52^{+1.53}_{-1.04}$ Gyr and $t_B = 2.02^{+0.99}_{-0.58}$ Gyr. For α Cen, we find $t_A = 4.67^{+1.19}_{-1.18}$ Gyr and $t_B = 4.29^{+0.33}_{-0.31}$ Gyr. Even with the generous inferred range of surface rotation due to differential rotation, the Barnes relation predicts ages that are systematically too young, especially in the case of α Cen B. This large discrepancy with old field binaries, coupled with its deviation from M37's median trend (Figure 6), indicates that the Barnes (2007) relationship does not reproduce observations. Better rotation measurements for the α Cen system to determine a true, rather than inferred, range of differential rotation are important for testing rotation-mass-age relationships. These examples underscore the fact that differential rotation imposes an uncertainty in rotation-based ages and we will return to this point in §3.2.2.

In addition to these binary systems, photometric monitoring programs have reported rotation periods for large samples of FGK (CoRoT, Affer et al. 2012) and M (MEarth, Irwin et al. 2011) field stars. Although these represent a heterogeneous stellar population that will include synchronized binaries as well as both dwarfs and subgiants, the rotation distribution gleaned by these studies still provides interesting constraints. These field star studies report rotation periods as long as 80–100 days for M–F stars. The existence of such slowly spinning stars presents a challenge to current rotation-mass-age relationships, if they are main sequence stars. Because subgiants are expected to have longer rotation periods than dwarfs, we recommend a cautious interpretation of field star observations that do not distinguish evolutionary state. The three gyrochronology relationships tested here all predict that a 100 day period corresponds to ages older than 10 Gyr within the color regime B–V< 1.5. Reiners & Mohanty (2012) recognize that their wind law is much too weak to explain the slowly rotating M stars from Irwin et al. (2011). To account for this problem, they change their saturation threshold from 8.5 days to $P_{\mathrm{crit}} = 40$ days below $M \leq 0.3$ M$_\odot$. They justify this break in the saturation behavior with an argument that the effective τ_{CZ} rises sharply at low masses (e.g. Stepien 1994; Kim & Demarque 1996; Kiraga & Stepien 2007). With this adjustment, the Reiners & Mohanty law reproduces the ~ 100 day rotation periods for M stars, but retains rapid rotaion for more massive stars. Even with the adjusted P_{crit}, the Reiners & Mohanty law cannot explain the recent detection of equally long rotation periods in K and G dwarfs (Affer et al. 2012). The modified Kawaler wind law also fails to predict 100 day periods. At 10 Gyr, our models predict a median rotation period of ~ 40 days for G dwarfs, dropping to ~ 70 days for M dwarfs. These long-period field stars will present a serious challenge to our understanding of angular momentum evolution if the period measurements prove to not be aliased and if further examination places these stars on the main sequence.

3.2. *Uncertainties in Rotation-Based Ages*

Until stars lose the memory of their initial conditions, we cannot distinguish between an inactive young star and an active older star at the same rotation period. This implies that there exists a minimum error in the mean rotation-mass-age relationship due to the intrinsic dispersion in stellar rotation rates. We quantify this minimum age uncertainty and evaluate in what mass and period regimes the rotation period becomes a good estimator of age for field stars (§3.2.1).

Furthermore, rotation period measurements suffer from uncertainties. While instrumental and observational errors may be removed by longer baseline monitoring or higher precision photometry, the fact that stars do not have a unique surface rotation period presents an irreducible uncertainty (see §4.1 for a possible exception). Seismic inversion (e.g. Schou et al. 1998) and observations of sunspots at different latitudes on the Sun's surface (e.g. Lustig 1983) agree that the solar rotation rate is significantly faster at the equator than near the poles. Because we cannot know if we are measuring equatorial rotation rates for unresolved stars, this sets bounds on the precision of rotation period, and therefore age measurements using this technique (§3.2.2).

We also consider how different modeling choices influence our derived uncertainties. Section 3.2.3 investigates the impact of choosing a broader metric to describe the spread in the rotation distribution. The uncertainty in the age of M37, which sets our initial conditions, introduces a systematic error in the age scale (§3.2.4). Due to uncertainties in color-temperature relationships, different stellar isochrones yield divergent mass scales for a cluster main sequence, particularly among red stars. Because the angular momentum evolution depends on the internal stellar structure, the adopted mass scale affects the evolution of the rotation distribution (§3.2.5). Finally, we examine the impact on rotation-based age uncertainties of using the two different angular momentum loss laws described in §2.4.

3.2.1. *Uncertainty Due to Initial Conditions*

For our base case, we adopt a modified Kawaler (1988) angular momentum loss model. We distill the M37 distribution into a mass-dependent median rotation period and use the interquartile region to measure of the period uncertainty due to the spread of initial rotation rates. We evolve the smoothed 25th and 75th percentile curves (defined in §3.1.1) forward in time until we reach either the age of the Galactic disk, which we take to be $t = 10$ Gyr, or when a model corresponding to that mass leaves the main sequence. Table 2 contains the 10th, 25th, 50th, 75th, and 90th percentile curves as a function of time, where $(B\text{–}V)_0$ and $T_{\rm eff}$ are computed at fixed mass using a YREC isochrone of the appropriate age and [Fe/H]=+0.045. Interpolation on this grid allows the determination of rotation-based ages and the associated uncertainty.

The top panel of Figure 9 shows an example of how the interquartile range changes over time at fixed mass. A horizontal cut across these curves gives the 25th and 75th period percentiles for a bin centered at $M = 0.60\ M_\odot$ at fixed age. In this calculation, the predicted range of rotation periods converges to a unique value at fixed mass and age. For field stars, it is useful to invert the problem and ask what range of ages is expected for a measured rotation period. This corresponds to taking a vertical cut through Figure 9, which gives the range in age predicted for a fixed rotation period. A unique rotation-mass-age relationship will predict a spurious range of ages for coeval stars born with different initial rotation rates because stars that are initially rotating faster take longer to reach a given period than initially slow rotators do. We take the difference between ages inferred from the top and bottom of our rotation distribution ($\Delta \log$ Age) as the uncertainty in the age estimate from gyrochronology (Figure 9). This ambiguity in age is a fundamental limitation of this technique; it takes a finite time for stars to forget their initial conditions. The lower panel shows the size of the age uncertainty for different measured rotation periods at fixed mass. The uncertainty in age declines toward longer periods because, if stars have time to spin down to long rotation periods, the rotation distribution will have had more time to converge.

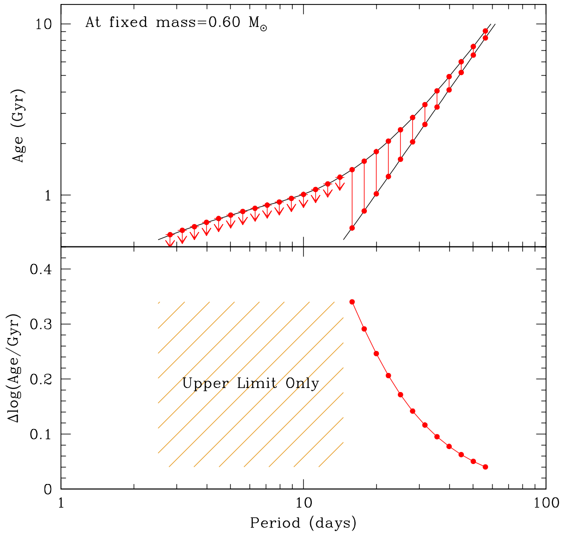

Fig. 9.— *Top:* Interquartile range of periods from M37 evolved forward using a solar calibrated Kawaler law for a bin of 50 stars centered on 0.60 $M_\odot$ (black lines). Vertical red lines cut the rotation profile at fixed period showing range of possible ages. Arrows indicate that gyrochonology can place either an upper limit on the age of a star with this period, but that it may be younger than 550 Myr; or, a lower limit, bounded by the age of the Galaxy. *Bottom:* Width of interquartile band as a function of period. The quantity $\Delta \log(\text{Age})$ gives the uncertainty in rotation-based age.

There exists a region where gyrochronology can only provide an upper limit on the age of a star. We define this to be the case if the measured period lies within the interquartile range of M37 at 550 Myr. We lack further information due to our choice of initial conditions, and we discuss rotation-age distributions in young stars in a companion paper (Paper II). Only $\sim 5\%$ of field stars should fall in the regime where only an upper limit is relevant, assuming the Galactic disk to be 10 Gyr old with a constant star formation rate. On the other end, at 10 Gyr, the period distribution still has some width and the slowly rotating quartile period sets a lower bound on the age and the upper bound is the age of the Galaxy.

Expanding our focus, we determine how the uncertainty in age depends not only on rotation period, but also on mass. In this ideal case, where we have assumed both perfect mass and rotation measurements, and that the theory fully encapsulates the physics of stellar angular momentum loss, the contours on the top panel of Figure 10 give the best possible constraints on age for each combination of mass and period, where lighter grays correspond to smaller $\Delta \log$ Age. The uncertainty in age increases towards lower mass because convergence takes longer for these stars. Gyrochronology can define an age range, rather than just place upper limits on the age, in the shaded region. In some windows of mass and period

TABLE 2
MEDIAN GYROCHRONOLOGY WITH UNCERTAINTIES FOR A MODIFIED KAWALER WIND LAW

Age (Gyr)	Mass ($M_\odot$)	$(B\text{–}V)_0$ (mag)	$T_{\rm eff}$ (K)	P_{10} (days)	P_{25} (days)	P_{50} (days)	P_{75} (days)	P_{90} (days)
0.55	0.45	1.54	3643	0.58	0.77	2.09	9.43	14.42
0.58	0.45	1.54	3644	0.59	0.79	2.14	9.65	14.77
0.63	0.45	1.54	3643	0.62	0.83	2.25	10.15	15.53
0.69	0.45	1.54	3642	0.66	0.87	2.38	10.71	16.39
0.76	0.45	1.54	3642	0.69	0.92	2.52	11.35	17.36
⋮	⋮	⋮	⋮	⋮	⋮	⋮	⋮	⋮

NOTE. — Table 2 is published in its entirety in the electronic edition of this journal. A portion is shown here for guidance regarding its form and content.

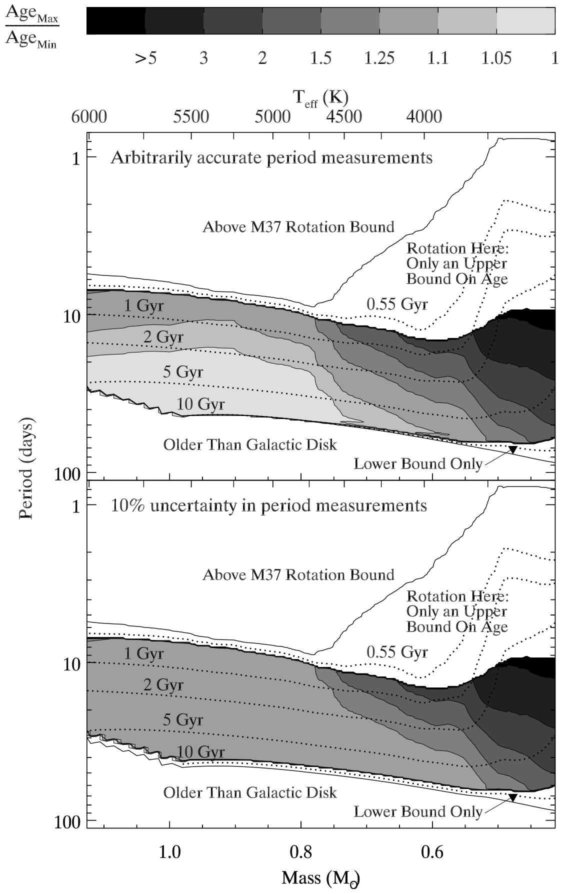

FIG. 10.— Uncertainty in age ($\Delta \log(\mathrm{Age/Gyr})$) as a function of measured period and mass. The shaded region shows where gyrochronology is valid for our models. Uncertainties in age are calculated in the same manner as for Fig. 9. Lighter grays correspond to better constraints on the rotation age. Dotted lines give the median rotation period as a function of mass when the M37 distribution is evolved to 0.55, 1, 2, 5, and 10 Gyr using a solar calibrated Kawaler wind law. The mass axis is converted to temperature above assuming a 1 Gyr, $[\mathrm{Fe/H}]_{\mathrm{M37}} = +0.045$ YREC isochrone. Both the panels assume that the solar calibrated Kawaler wind law perfectly captures the physics of angular momentum loss in cool stars and that masses can be measured to arbitrary precision. The upper panel assumes that rotation periods can also be perfectly measured, while the lower panel imposes a minimum 10% uncertainty in the period measurement.

space, constraints tighter than $\Delta \log(\mathrm{Age}) \sim 0.05$ dex are possible, assuming perfect period measurements. As before, the region where gyrochonology can only provide an upper limit on the age arises from the initial spread in rotation rates. The lower bound occurs because we halted the simulation after 10 Gyr. The upward slope of the lower boundary at high mass represents these stars evolving off the main sequence. We offer the following cautions when interpreting this figure. First, because we use the interquartile region as our measure of the width of the rotation distribution, there will be stars that lie outside this range. Second, the specific values of the period and age uncertainty depend on the validity of the underlying angular momentum evolution model.

3.2.2. *Impact of Latitudinal Differential Rotation and Period Errors*

Unfortunately, achieving these theoretical limits may not be feasible with real stars. In §3.1.3, we demonstrated that old field stars have a significant range in measured surface rotation rates which reflects latitudinal surface differential rotation. This provides an additional fundamental source of uncertainty in rotation-based ages: where on the surface is the rotation period being measured?

If the Sun's differential rotation is characteristic of solar type stars, then the latitude of a star spot could significantly impact the measured rotation period. Although the range of rotation periods may be as large as 30% of the mean rotation period (Donahue et al. 1996), we consider a more conservative case where latitudinal differential rotation only sets a 10% range in rotation period. To account for this, we therefore broaden our interquartile range by taking

$$\Delta \log P = \max\left(\log \frac{P_{75}}{P_{25}}, \frac{\sigma_P}{P \ln 10}\right) \tag{7}$$

where $\sigma_P/P = 10\%$ is the minimum set by differential rotation. When widening the distribution beyond the ratio of quartile periods, we centered $\Delta \log P$ on the geometric mean of the quartile rotation periods. We then repeat the process described above to obtain the plot shown in the bottom panel of Figure 10. Comparison between the upper and lower panels shows that, even given a perfect angular momentum loss theory, latitudinal differential rotation at this level sets a floor on the age precision from gyrochronology estimates instead of allowing the range of rotation rates to converge arbitrarily.

The impact of surface differential rotation is most severe in more massive and older stars. For example, if a 0.5$M_\odot$ star has a rotation period of 11.5 days, gyrochronology can only constrain its age to a factor of 4.7 regardless of whether there is a minimum precision in period. Meanwhile, the age of a 0.8 $M_\odot$ star with a period of 40 days can be tightly constrained to 2% with perfect period measurements, but only to 20% when we include a 10% range due to differential rotation. For the Sun's mass and equatorial rotation period, its age can be constrained to 2% with perfect period measurements. With this correction for differential rotation, the Sun's age is predicted to lie between 4.07 and 4.85 Gyr. Generally, imposing a 10% range in rotation periods translates to a 20% uncertainty in age.

The dotted curves in Figure 10 delineate the median rotation period at a selected set of ages. At 550 Myr and 10 Gyr, rotation only sets a bound on the stellar age. At intermediate ages, the median rotation period may be mapped onto a typical uncertainty for a star of a given age. Although the logarithmic scale from Figure 10 is useful for visualizing the fractional error, the absolute age error also provides a helpful comparison. The solid lines in Figure 11 trace the absolute age uncertainties for stars with the median rotation period at select ages. Given arbitrarily accurate rotation period measurements, stars more massive than 0.75 $M_\odot$ always have an uncertainty in age smaller than 270 Myr. Adding in a 10% uncertainty in rotation period has the effect of capping the age precision at around 0.38, 1, or 1.5 Gyr for a 2, 5, or 8 Gyr population, respectively. The absolute age uncertainties are smallest for younger stars, but become increasely larger for older stars. Nonetheless, the absolute age uncertainty is always below 2 Gyr for stars with $M > 0.52$ $M_\odot$. The wide binaries 61 Cyg and α Cen corroborate this expected level of uncertainty in rotation-based ages due to latitudinal surface differential rotation (§3.1.3).

3.2.3. *Impact of Choice for Metric for Distribution Width*

In §3.1.1, we describe the width of the rotation distribution by the interquartile region. One might argue that this is too restrictive and does not capture the full range of the distribution. We therefore investigate the impact of choosing a more generous metric, the range of rotation rates between the 10th and 90th percentile, to characterize the rotation distribution.

We compare the absolute age uncertainties in Figure 11. The largest differences occur for low mass stars, where the spread in rotation rates is maintained until late times. The metric chosen to describe the rotation width does not change the functional form. Even if arbitrarily accurate period measurements are possible, differences in the age uncertainty are only a few hundred Myr for stars on the tightly converged mass-rotation sequence. From the bottom panel, we see these differences due to the choice of width metric are smaller than the age uncertainty due to differential rotation for stars with $M > 0.8$ $M_\odot$ at 2 Gyr and to even lower masses for older stars. We therefore consider the interquartile region a fair characterization of the rotation-based age uncertainty.

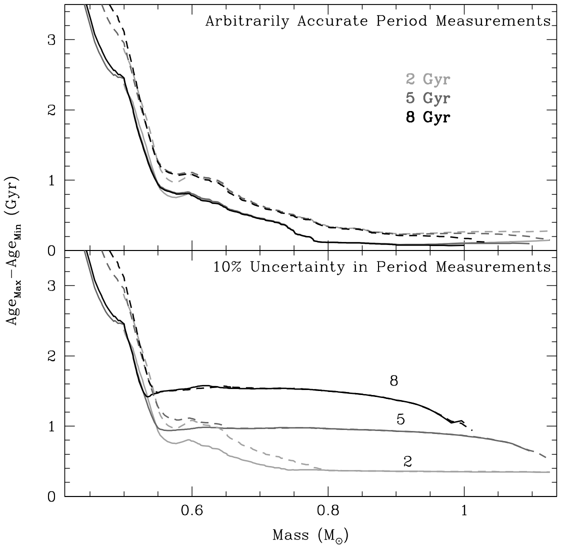

FIG. 11.— Absolute age uncertainty as a function of mass for a star with the median rotation period at age 2, 5, and 8 Gyr (light to dark). Solid lines correspond to using the inner 50% of stars to measure the distribution width while dashed lines indicate the inner 80% of stars. The top panel assumes rotation periods are measured with arbitrary precision, while the bottom panel includes a 10% uncertainty in period measurements.

3.2.4. *Impact of the Age Scale*

Uncertainties in the absolute age assigned to M37 affect all of our derived rotation-based ages. In §2.1, we initialize all models to the age of M37 determined from Hartman et al. (2008). By fitting isochrones to the cluster main sequence, Hartman et al. measured an age of 550 ± 30 Myr. To see how this uncertainty in the initial conditions maps onto our age predictions, consider the illustrative case of Skumanich spin down. In that scenario, the rotation rate scales as $\omega \sim t^{-0.5}$. This implies that:

$$\frac{t_\bigstar}{t_{\mathrm{M37}}} = \left[\frac{\omega_{\mathrm{M37}}}{\omega_\bigstar}\right]^2. \tag{8}$$

Thus, the age of M37 (t_{M37}) enters linearly into the calculation of a star's age ($t_\bigstar$). An analogous calculation may be performed for both the Kawaler and the Reiners & Mohanty wind laws. As such, the ±5% uncertainty in the age of M37 (Hartman et al. 2008) propagates to a ±5% uncertainty in the ages predicted by these models. This uncertainty in the scale factor represents a systematic uncertainty for any semi-empirically calibrated model. The random error associated with the age of any particular cluster may be reduced by using many different clusters. However, the systematic uncertainty in the overall open cluster age scale will remain.

3.2.5. *Impact of the Mass Scale*

The wind law describes the angular momentum loss rate in terms of mass, rather than an observable quantity like color. Stellar interior models predict divergent mass-color relationships, particularly at the cooler end. As described in §2.1, we convert measured $(V{-}I_C)_0$ to mass using both YREC and Padova isochrones. Figure 1 shows that both isochrones agree well for $(V{-}I_C) < 1.2$, but diverge for redder stars. For $(V{-}I_C) > 1.2$, Padova isochrones map stars of a particular color onto a lower

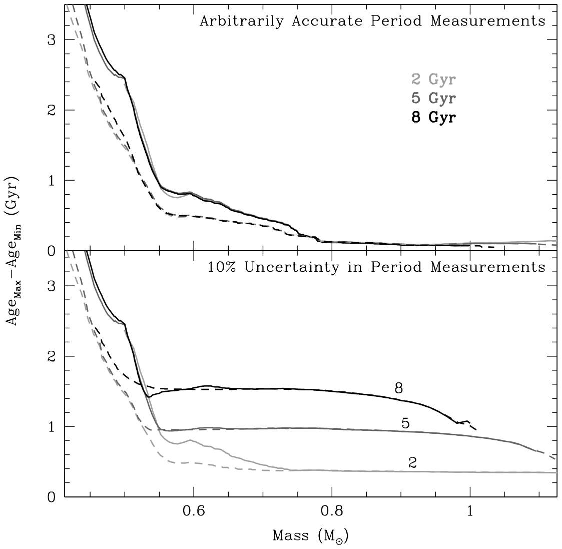

FIG. 12.— Absolute age uncertainty as a function of mass for a star with the median rotation period at age 2, 5, and 8 Gyr (light to dark) calculated with YREC (solid) and Padova (dashed) isochrones. The top panel assumes rotation periods are measured with arbitrary precision, while the bottom panel includes a 10% uncertainty in period measurements.

mass than YREC isochrones do. Since both isochrone systems are widely used for color-temperature conversions, we investigate how this affects the age uncertainties.

We use the Padova isochrones to define the mass scale for the M37 initial mass-rotation distribution and repeat the calculations described in §3.2.1. This will have two effects on the rotation-mass-age distribution. First, using the Padova isochrones should result in a shift of red stars to lower masses. Second, the absolute mass scale affects the rate of angular momentum loss because it changes the star's interior structure, affecting the moment of inertia and leading to a different spin down history.

The absolute age uncertainty derived from the Padova isochrones is compared with the YREC results in Figure 12. Above 0.77 $M_\odot$, the Padova and YREC isochrones produce identical constraints. Below that, the Padova isochrones appear to be a stretched version of the YREC isochrones. Because the Padova isochrones translate a red color to a lower mass, the Padova curves extend to lower masses than the YREC ones do. As a result of the stretched mass scale, Padova isochrones predict tighter age constraints than YREC does for a given mass and period.

Although the exact value of the age uncertainty depends on the isochrones used to determine the mass scale, the difference is confined to the low mass regime and, even there, the Padova contours retain the qualitative characteristics of the YREC contours. While these similarities are reassuring, it is important to carefully consider how to map observed colors onto mass. In Figure 1, it is apparent that the YREC isochrones better reproduce the shape of the cluster main sequence. For this reason, we favor the YREC isochrones for this study.

3.2.6. *Impact of the Choice of Angular Momentum Loss Law*

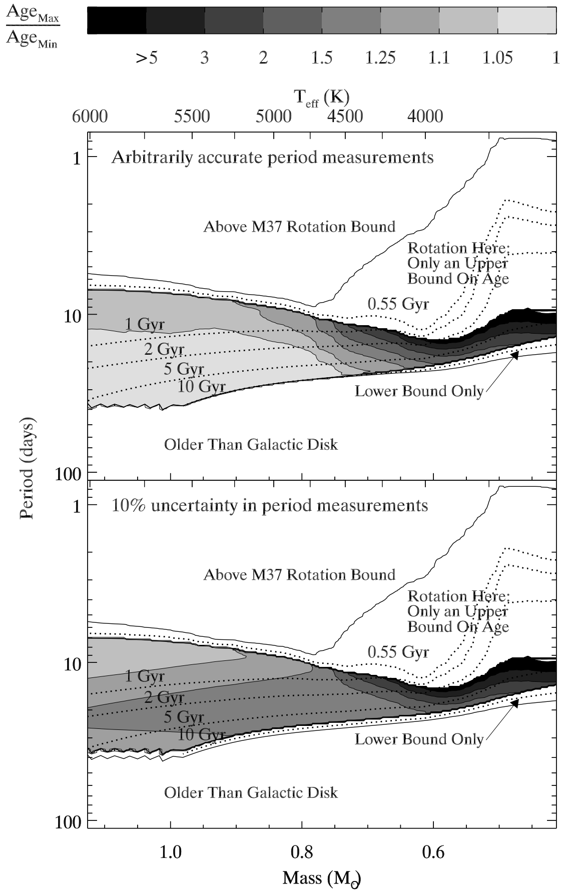

FIG. 13.— Uncertainty in age ($\Delta \log(\mathrm{Age/Gyr})$) as a function of measured period and mass, where the initial mass distribution was calculated using YREC isochrones and evolved forward in time with the Reiners & Mohanty (2012) braking law. The upper panel assumes that rotation periods can also be perfectly measured, while the lower panel imposes a minimum 10% uncertainty in the period measurement. See Figure 10 for an explanation of other markings.

Thus far, we have used the widely-adopted Kawaler (1988) prescription for angular momentum loss, modified to include a Rossby-dependent saturation threshold as described in §2.4.1. While this simple model reproduces observations well in the open cluster domain; there is limited data for older field stars. Alternative formulations should therefore be explored, and the Reiners & Mohanty prescription is an intriguing choice.

Following the procedure described in §3.2.1 with the Reiners & Mohanty wind law produces the fractional age uncertainty contours displayed in Figure 13. The Reiners & Mohanty braking law introduces some interesting features that merit closer examination. Because the Reiners law enforces rapid rotation among low mass stars until late times, rotation provides only a weak constraint on age. For stars with M$>$ 0.6 $M_\odot$, rotation-based ages cannot be pinned down to better than 50%, regardless of the precision of rotation period measurements. Among higher mass stars, Reiners & Mohanty predict rapid angular momentum evolution until $\sim$ 700 Myr. If a star is caught with a rotation period in this range, its age may be determined to a precision of about 7% (or approximately 30-50 Myr). Imposing a 10% period measurement error (Figure 13, bottom panel) pro-

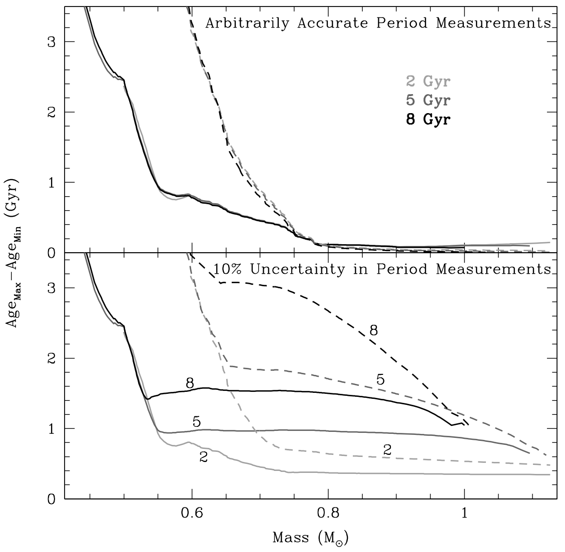

FIG. 14.— Absolute age uncertainty as a function of mass for a star with the median rotation period at age 2, 5, and 8 Gyr (light to dark gray) calculated with Kawaler (solid) and Reiners & Mohanty (dashed) braking law. The top panel assumes rotation periods are measured with arbitrary precision, while the bottom panel includes a 10% uncertainty in period measurements.

duces a sweet spot for stars with rotation periods around 10 days.

Figure 14 shows the absolute age uncertainty predicted by both the Kawaler and Reiners & Mohanty braking laws. When measurement uncertainty is introduced in the bottom panel, the Reiners & Mohanty law predicts degraded precision in old stars because the Reiners & Mohanty law has a weaker rate of angular momentum loss than the Kawaler law does at ages > 1 Gyr (see Figure 2). Both exhibit stable rotation-based age uncertainties with mass down to a critical point where the age uncertainty abruptly becomes quite large, corresponding to the point of convergence. This effective boundary to the rotation-based age technique is dramatically shifted 0.15 $M_\odot$ higher with the Reiners & Mohanty law. This shift is due to the mass-independent way that Reiners & Mohanty treat magnetic saturation. Comparison of Figures 3 and 4 shows that Reiners & Mohanty set the saturation threshold lower than the Rossby scaled saturation threshold for $(B\text{–}V)_0 < 1.4$ ($M \gtrsim 0.57\ M_\odot$). This keeps stars in the saturated regime longer than with a Rossby scaled saturation threshold. Because a Rossby-scaled saturation threshold is supported by observations of open clusters (see 2.4.1), we consider the Kawaler version to be a more realistic boundary to the rotation-based age technique.

Because the rotation-based age constraints differ strongly between these two angular momentum loss laws, properly testing the rate of angular momentum loss is important. For now, we favor the modified Kawaler wind law because it properly reproduces Skumanich spin down at late time for solar type stars and it incorporates a Rossby scaled wind law, both of which are supported by open cluster observations. Additionally, the Reiners & Mohanty law fails to reproduce the open cluster distribution, as seen in their Figure 4. They predict rotation periods that are too long compared to the cluster M50 for $M < 0.8\ M_\odot$. They argue that this is due to core-envelope decoupling, which is not included in their modeling. This can explain the presence of slow rotators over the mass range where core-envelope decoupling is expected to be important, primarily for solar-like stars with shallow surface convection zones. However, low mass stars (below 0.5-0.6 $M_\odot$) are well described empirically with solid body spin down models (Tinker et al. 2002). The striking differences between their models and cluster data for cool dwarfs therefore cannot be explained by this phenomenon. The modified Kawaler braking law developed in response to problems in reproducing empirical trends, and a comparable modification of the Reiners & Mohanty (2012) prescription could be viable and interesting to explore.

3.3. *Amplitudes and Age Uncertainty*

As demonstrated in the previous section, a regime exists where the range of stellar rotation rates has converged enough to make gyrochronology a good clock. For stars of the same mass, the age constraints from gyrochronology are tighter for more slowly rotating stars. Because magnetic activity, and therefore the presence of starspots, declines with time, so too does the amplitude of photometric variability. This raises the question of whether there exists a good mass window where stellar amplitudes of variability are high enough that current ground based surveys can obtain rotation periods for the older, less magnetically active stars that are the most promising candidates for gyrochronology. In the following discussion, we demonstrate that current ground based studies can measure rotation-based ages for stars up to 1-2 Gyr.

From the ground, current rotational studies have a minimum detectable amplitude of 3 millimag (e.g. Hartman et al. 2009; Meibom et al. 2011a), which may be pushed to as good as 1 millimag in the future. The space-based Kepler mission is monitoring roughly 150,000 stars with a time cadence of 30 min. Its photometric precision is estimated to be 1 millimag for a 15.5 mag star and as good as 10^{-5} mag for an 8^{th} mag star[2]. Indeed, some studies of stellar amplitude from the first quarter of Kepler data (e.g. Basri et al. 2010, 2011) have already begun examining how the amplitude of variability depends on T_{eff}, periodicity, and plan to investigate the age distribution of these stars once a longer time baseline is available.

In light of these upcoming developments, we use the current observations from open clusters to estimate what trends should be visible in the Kepler sample. To do so, we require a conversion between rotation period and amplitude. Hartman et al. (2009) used the clean sample of rotation periods in M37 to explore the relationship between observed amplitude of variation and Rossby number. Dividing their sample at $(B\text{–}V)_0 = 1.36$, the blue stars display a strong anti-correlation between Rossby number (R_0) and amplitude which flattens out for $R_0 < 0.3$. Redward of that division, the anti-correlation is less pronounced and the constraints on the convective overturn timescale are weaker. Focusing on the bluer stars, Hartman et al. call into question the period measurements for stars with $R_0 > 0.6$, raising the possibility

---

[2] http://keplergo.arc.nasa.gov/CalibrationSN.shtml

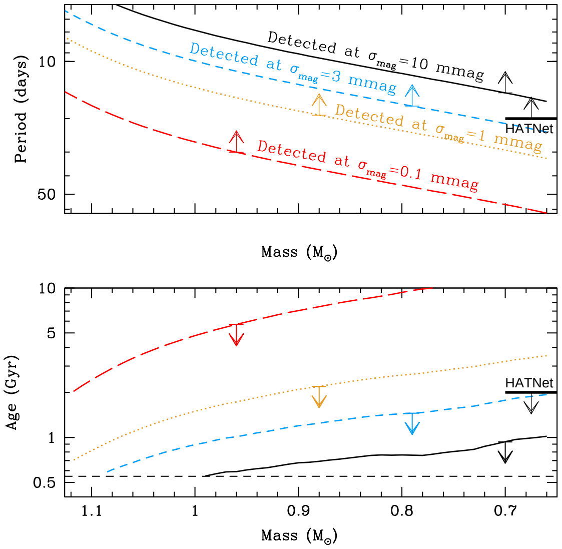

FIG. 15.— *Top:* Maximum observable rotation period for a survey capable of detecting amplitude variations of 10 (black; solid), 3 (black; short dash), 1 (gold; dot), and 0.1 (red; long-dash) millimag. *Bottom:* The associate median age of a star with maximum period given in the top panel. Each line represents the maximum age a survey of a given precision could expect to obtain via gyrochronology. Arrows indicate the direction of the trends. The 550 Myr age bound is shown as the horizontal black dashed line. The HATNet survey (black bar) is capable of detecting the rotation periods of 20 days at amplitudes of 0.01 mag, which corresponds to ages of 2 Gyr or younger.

that they reflect spot evolution timescales rather than rotation periods. Based on this, Hartman et al. find an empirical fit to the r-band amplitude of M37 cluster members with (B–V)$_0$ < 1.36 and $R_0 < 0.6$ of the form

$$A_r = \frac{0.078 \pm 0.008}{1 + \left(\frac{R_0}{0.31 \pm 0.02}\right)^{3.5 \pm 0.5}}. \tag{9}$$

We invert Eq. 9 to determine the maximum observable rotation period for a survey of a given photometric precision. For some amplitude A_r, the resulting R_0 may be converted into a rotation period if the τ_{CZ} is known. We perform this calculation for a grid of different stellar masses where we utilize the τ_{CZ} predicted by the YREC models. Because τ_{CZ} changes only very slightly over a star's main sequence lifetime, we adopt a mass-τ_{CZ} relation at 1 Gyr. We restrict the grid to the range where the Hartman et al. relationship is applicable. To determine this, (B–V) is converted to mass using a 1 Gyr, $[\mathrm{Fe/H}]_{M37} = +0.045$ YREC isochrone. Under this transformation, the color limit (B–V)$_0$ < 1.36 corresponds to masses M> 0.65 M$_\odot$. This results in a mass-period relationship at fixed amplitude. These iso-amplitude curves represent the longest period for which a star of that mass could be detected with that photometric precision. A more slowly rotating star tends to have smaller variability in accordance with the activity-rotation-age relationship and therefore will drop below a given detection threshold.

These lines of maximum period are shown in the top panel of Figure 15. Because older stars rotate more slowly, if a survey is unable to detect periods longer than some threshold, this places an upper limit on the age of stars that can be determined with gyrochronology for that survey. We translate the maximum rotation periods into age using the median of the rotation distribution at a grid of ages given in Table 2. The mass range of these calculations is set by where Eq. 9 is applicable and by the scarcity of high mass stars in M37.

These maximum ages, shown in the bottom panel of Figure 15, indicate that the current photometric precision of ground-based surveys (3 millimag) limits gyrochronology to measuring stars younger than ∼ 1 − 2 Gyr. An improvement of a factor of 3 in precision (∼ 1 millimag) would open up the possibility of measuring rotation-based ages for stars as old as 2 − 3 Gyr. A further order of magnitude improvement in precision is required to use gyrochronology to measure the ages of stars over the full age range of the Galactic disk (up to 10 Gyr). Kepler is capable of achieving the requisite precision to do so for stars brighter than $\mathrm{m}_{\mathrm{Kep}} \sim 11$ mag (Basri et al. 2010).

The R_0-amplitude relationship suffers from a very limited dynamic range in R_0 from the M37 data. New observations of field stars will extend the relationship to larger R_0 (longer rotation periods) and provide a better constraint on the unsaturated slope. For now, we motivate a relationship with a shallower slope and consider its ramifications. This analysis is based on the Hartman et al. best fit curve that maps R_0 to amplitude. Some of the scatter in the M37 data is stochastic. The amplitude of variability of a star depends not only on the spot covering fraction, but also on the degree to which the spots are isotropically distributed over the surface of the star. At one extreme, if a star had a perfectly isotropic distribution of spots, no modulation in the light curve would be observed. Alternatively, large amplitude modulations would arise in the case of a concentration of spots along one line of longitude. By this logic, the upper envelope of the amplitude-R_0 diagram for M37 (see Figure 17, Hartman et al. 2009) represents the maximum possible amplitude of variability for a star of a given R_0. The cloud of points under this envelope could be produced by different spot configurations that decrease the amplitude of variation. If instead we had used the upper envelope, rather than the best fit through the cloud of points, to define the the transformation from R_0 to amplitude, visual inspection indicates that the slope of the anti-correlation would be shallower. If this is the case, then using the best-fit R_0-amplitude relationship would represent an underestimate of the amplitude of variability. That is, there may be older, more slowly rotating stars which exhibit higher amplitude variability than one would expect from Eq. 9 because they possess a more favorable configuration of spots. This would enable ground-based surveys with sufficiently long time baselines to probe older ages than predicted in Figure 15. Conversely, stellar variability may be suppressed to arbitrarily low levels by an nearly isotropic distribution of spots and therefore one should not expect all low amplitude stars to be old.

We can perform an empirical check on these maximum period-age-sensitivity predictions using current field star data. Hartman et al. (2011) searched for stellar variability in light curves collected by the HATNet survey for transiting extrasolar planet. This yielded rotation periods for 1568 field F, G, K, and M dwarfs. HATNet offers a photometric precision of a few millimag for $R_C \sim 8$

mag and 0.01 mag for $R_C \sim 12$ mag. Figure 18 in Hartman et al. (2011) compares the mass-rotation distribution for field stars detected with HATNet with those from open clusters, including M37. At 0.7 $M_\odot$, the field stars have rotation periods a factor of ~ 2 longer than the corresponding stars in M37. This also agrees with Hartman et al.'s Figure 17 that shows that the number of detected stars rises slowly as a function of rotation period, peaks around 20 days, and then drops off steeply to larger periods for all color bins. If HATNet can detect rotation periods of ~ 20 days or shorter, this corresponds to ages K-star ages 2 Gyr or younger from interpolation on Table 2. We overplot the HATNet detection capabilities in Figure 15 and discover that they more closely match the curve at $\sigma_{\rm mag} = 0.003$ mag than the 0.01 mag curve that corresponds to the surveys detection threshold. This is an encouraging sign that our predicted detection limits are actually too pessimistic and the activity-rotation-age relationship does not fall off as steeply as Equation 9 predicts.

The results from HATNet mean that current ground-based surveys can identify populations of stars younger than 2 Gyr based on their amplitude of varability alone. However, such a sample could suffer contamination from merger products or synchronized binaries that are more active than isolated field stars of the same age. Additionally, the detection efficiency among slowly rotating is unknown. Stars inclined pole-on to our line of sight or those at the minimum in their stellar activity cycle contribute to a non-detection fraction of stars at a given period. The impact of these stellar population effects will be discussed in §4.

4. DISCUSSION AND CONCLUSIONS

Our goal is to quantify the strengths and weaknesses of rotation as a stellar age indicator. For which stars is rotation a good chronometer, and how reliable are those ages likely to be? How does it compare to other age diagnostics? Rotation decays as stars age, and old stars are therefore harder to detect than young stars. How does the age limit for photometric surveys depend on the precision of the photometry? In addition to these questions, there are broader issues that deserve comment. Our data is concentrated in young stars, while the most promising applications are for old stars. What potential issues could complicate the interpretation of rotation in older stars? How can observational selection effects be accounted for? And what backgrounds need to be understood for stellar population studies? In our summary we begin with the quantifiable answers to the first class of issues, and then turn our attention to the challenges and opportunities for progress in the future.

4.1. *Current Results*

Our main result is that stellar rotation is a promising tool for estimating the ages of Sun-like stars. The upper mass limit for rotation-age relations is set by the F star transition from deep to shallow surface convection zones. It is not clear that stars more massive than $M \simeq 1.2$ $M_\odot$ have a rotation-age relationship, and it is difficult to detect rotation periods signals for stars more massive than the Sun because the fractional star spot coverage, and the amplitude of variability, drops steeply for hotter stars.

We demonstrated the method of deriving rotation-based ages from spin down models works for stars below the F star transition and above the fully convective limit. Although both theoretical angular momentum loss models and the semi-empirical published gyrochronology relationships are calibrated to the same open cluster data, systematic errors arise in the extrapolation of these relationships forward in time. Because of the limited data at late times, constraining the rotational behavior of old stars is difficult. We find that both a modified Kawaler law and the Mamajek & Hillenbrand (2008) gyrochronology relation agree with constraints from old field binaries, although their predicted ages at fixed rotation period differ by as much as 30%. We view this as a measure of the current systematic error level in rotation-age relations.

These loose constraints from old binary stars opens the door for other angular momentum loss laws offering a different spin down trajectory than the modified Kawaler law. A reassessment of the 24 year old Kawaler braking law in the modern context is welcome. However, the proposed Reiners & Mohanty (2012) is inconsistent with data. Taking the Reiners & Mohanty (2012) law at face value indicates that there are a strong mass- and radius-dependent trends in the spin down behavior at fixed $\omega_{\rm crit}$. The torque is predicted to be so inefficient that it conflicts with long period rotation measurements from the old binary star systems (61 Cyg and α Per), and field K and M dwarfs from CoRoT (Affer et al. 2012), MEarth (Irwin et al. 2011), and Mount Wilson survey (e.g. Donahue et al. 1996). Future physically motivated revisions to the Reiners & Mohanty law may solve these problems. The Barnes (2007) relation is also inconsistent with the binary star data. More rotation and age data is necessary for old stars to provide better guidance to theory.

The age errors for gyrochronology relationships are larger than optimistic early claims. We investigated the impact of the range of stellar birth rates and surface latitudinal differential rotation on the precision of age measurements. These two phenomena will induce noise in age estimates of coeval stars even given perfect knowledge of the mean age-rotation relationship. Below 0.6 – 0.7 $M_\odot$, the minimum errors in rotational ages rise steeply; a range of surface rotation rates persists even for old stars. The exact boundary depends on how the period data is transformed from the observational (color, period) domain into the theoretical (temperature, mass, age) domain. Fortunately, there is good empirical guidance for both the time evolution of rotation and the proper choice of color-temperature relationships for low mass stars. There is thus a window in the 0.6 – 1.2 $M_\odot$ domain where stellar rotation is a promising chronometer.

Our technique for assigning errors for ages derived from rotation is conservative, and it may be possible to extract useful statistical age information from rotation in M dwarfs. The first step would be to empirically measure the shape of the rotation distribution and to empirically calibrate the time dependence of the spin down in systems of known age, such as open clusters. One could then construct a probability distribution of ages for a fixed rotation period. In any given field, however, the true probability distribution would be a function of the age distribution in the background. A good example would be a field with a star cluster superposed on a sparse background. A blind method would assign a range of ages to an intrinsically peaked age distribution. The age distribution in a given field would therefore need to be obtained independently (for example, with rotation-based ages of K stars) and a star by star age estimate could then be constructed for a sample of M dwarfs for which age estimates are otherwise difficult. This method would also be particularly useful for determining the ages of special targets, like planet hosts.

Stars like the Sun do not have a unique surface rotation rate, and this injects another source of uncertainty in rotational age. The latter effect becomes dominant in old field stars, imposing a minimum uncertainty of 20% in age estimates for a 10% range in surface rotation period. Different asymptotic angular momentum loss prescriptions have a major impact on the limiting precision, with the recent Reiners & Mohanty prescription implying much larger age uncertainties than previous spin down models based on a modified Kawaler (1988) loss law. A proper empirical calibration of the late-time dependence should address the functional form of the rotation-age relationship, and it will also serve as a check on the width of the observed distribution. A proper calculation of the impact of surface differential rotation on period measurements would involve modeling of the number and latitude distribution of spots as a function of starspot cycle, and our method may overestimate the practical impact of surface differential rotation. A larger problem may be the poor visibility of solar analogs during minima in their activity cycles (see below.) Because the timescale for stellar activity cycles is of order decades, monitoring over many seasons (e.g. the Mount Wilson survey) would be necessary to measure a stars' full range in surface rotation periods. Nonetheless, surface differential is not a fundamental limitation in the same way as the initial conditions are. With extremely long term monitoring, surface differential rotation could in principle be calibrated out. In such a case, one might define a equatorial rotation period-mass-age relationship. However, the time investment to do this for a large number of calibrating stars is significant.

We also examined prospects for using rotational variability to detect young populations from ground-based surveys. Current large ground-based surveys can reach a precision of 0.01 mag, and targeted open cluster campaigns have demonstrated 0.003 mag precision levels. We find that field K star populations younger than 1 and 2 Gyr (respectively) can be detected at these levels of precision if we adopt the amplitude-Rossby scaling relationship of Hartman et al. (2009). The field star data of Hartman et al. (2011) detected longer periods than would be predicted based on this estimate, suggesting that ground-based surveys may be capable of finding older stars than we predicted (2 Gyr at 0.7 $M_\odot$ and 0.01 mag precision, as opposed to our 1 Gyr estimate). Much higher levels of precision, currently only possible with satellite data, are required to detect rotational modulation in old stars. With new ground-based surveys on the horizon, such as LSST and the Las Cumbres Global Telescope Network, the monitoring large fractions of the sky will reveal variability for large samples of field stars. Because the amplitude of variability, like rotation rate, declines with age, such surveys will be able to identify all young K stars by variability alone. A subset of active G stars will also be discovered, consisting of a very young (< 1 Gyr) sample and tidally synchronized binaries.

4.2. *Cautions and Future Prospects*

Our method implicitly assumes that we can safely project the observational pattern seen in young systems into the future. There are interesting theoretical classes of models where this is not the case. For example, stars could vary in their core-envelope coupling because of differences in internal magnetic field morphology (Charbonneau & MacGregor 1993). This would lead to a persistent range in rotation rates at late ages generated by star-to-star differences in core rotation and the effective moment of inertia subject to spin down. It may not be possible to maintain a dynamo if the rotation rate becomes too long relative to the convective overturn timescale (Durney & Latour 1978); both spin down and starspots could simply cease in stars above some critical age for a given mass. Finally, gravitational settling could induce a composition gradient sufficient to decouple the surface convection zone from the interior. There is some evidence from old open clusters (Sestito & Randich 2005) that the pattern of lithium depletion stalls for systems older than a Gyr; if rotational mixing is tied to angular momentum loss (Pinsonneault et al. 1998), this could be evidence that there is a similar phenomenon in the torque. These questions can be addressed with Kepler data in old open clusters and targets with known seismic ages and measured rotation rates.

Interpreting rotation in field stars will also require careful consideration of observational selection effects and stellar population backgrounds. It will be difficult to detect stars observed nearly pole-on (Krishnamurthi et al. 1998; Hartman et al. 2010; Jackson & Jeffries 2010). It will also be difficult to detect solar-like stars either at the minimum of their sunspot cycle or if they are in extended Maunder minimum-like epochs. What is even more challenging will be modeling the stochastic effects of the distribution of star spots on the surface and observational selection effects from the observing cadence. All of these effects conspire to produce a substantial population of non-detections, and careful work will need to be done to quantify their impact.

Finally, our age estimates, as well as the body of gyrochronology work, assumes that we have a sample consisting of main sequence single stars. There will be significant background populations of tidally synchronized binaries and blue stragglers. A few percent of solar-type stars are likely to be merger products (Andronov et al. 2006), and their rotation rates will not be simple functions of their age. Subgiants may be difficult to distinguish from dwarfs, especially for F and G stars, and their rotation-age relationships will be very different from one another. All of these backgrounds will produce spurious signals when mapped onto single star relationships. Finally, the metallicity dependence of spin down relationships is poorly understood because the calibrating open cluster sample has a very limited dynamic range in composition.

4.3. *Gyrochronology in Context*

Using rotation as a clock is useful if it is competitive with other techniques for determining ages for unevolved

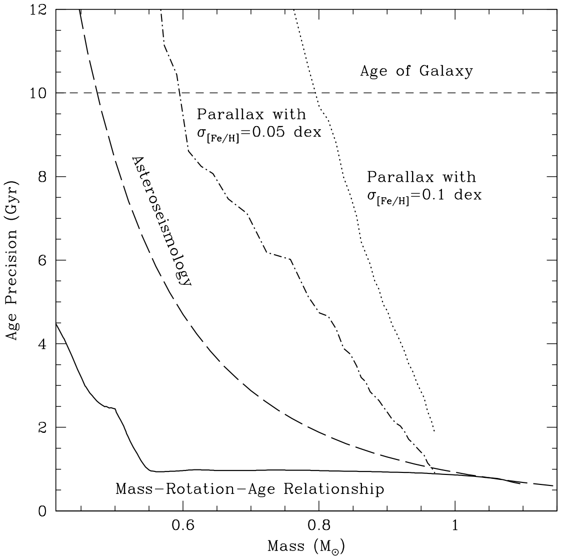

FIG. 16.— Comparison of expected age precision for a 5 Gyr old star from different techniques of estimating the age of main sequence stars below the turnoff. The contenders include rotation based ages (solid), asteroseismology (dashed), and trigonometric parallax combined with [Fe/H] measurements good to 0.1 dex (dotted) and 0.05 dex (dot-dash).

dwarfs. Ages may be determined by comparing a star's location on the CMD to stellar interior model predictions if the distance and metal content of a star is known. Gaia will provide exquisite geometric parallax measurements accurate to a few μas for $\sim 10^9$ stars. However, without helium or metallicity information, stellar isochrones suffer a degeneracy with age. Figure 16 shows the possible age precision achievable with [Fe/H] good to 0.1 and 0.05 dex, optimistically assuming perfect distance, temperature, and helium measurements. To generate these curves, we use Dartmouth isochrones to determine what difference in age produces a change in luminosity equivalent to a shift of ±0.1 dex (or 0.05 dex) in [Fe/H] at fixed temperature. Gaia's photometric accuracy will make the precision of metallicity information the limiting source of error.

With the advent of Kepler, asteroseismology is experiencing a renaissance. Asteroseismology obtains age estimates for dwarfs by measuring the helium content. These are good to 10% of a star's main sequence lifetime (Kjeldsen et al. 2009), making the best age constraints possible for more massive stars. Figure 16 shows that asteroseismology potentially offers better age constraints than isochrone-based techniques in the low mass regime. However, stellar pulsations may not even be detectable in low mass stars (e.g. Chaplin et al. 2011).

Because both geometric parallax and asteroseismology measure ages based on changes on the nuclear timescale, both suffer higher uncertainties for low mass stars. In comparison, Figure 16 demonstrates that rotation consistently offers ages good to $\sim$ 1 Gyr for stars M> 0.55 $M_\odot$. Rotation-mass-age relationships are not competitive with other techniques for stars more massive than the Sun and the spread in rotation is large for low mass stars. Nonetheless, in an intermediate mass regime, rotation-based ages are not only competitive, but clearly the best possible age indicators available for field dwarfs.

We are grateful to Donald Terndrup for his thoughtful comments and illuminating discussions in the preparation of this manuscript. C.E. and M.P. were supported by NSF grant AST-0807308 to The Ohio State University.

REFERENCES

Affer, L., Micela, G., Favata, F., & Flaccomio, E. 2012, arXiv:1202.4947
Allain, S. 1998, A&A, 333, 629
van Altena, W. F., Lee, J. T., & Hoffleit, E. D. 1995, New Haven, CT: Yale University Observatory, —c1995, 4th ed., completely revised and enlarged,
Andronov, N., Pinsonneault, M. H., & Terndrup, D. M. 2006, ApJ, 646, 1160
Attridge, J. M., & Herbst, W. 1992, ApJ, 398, L61
Barnes, J. R., Collier Cameron, A., Donati, J.-F., James, D. J., Marsden, S. C., & Petit, P. 2005, MNRAS, 357, L1
Barnes, S. A. 2007, ApJ, 669, 1167
Basri, G., et al. 2010, ApJ, 713, L155
Basri, G., et al. 2011, AJ, 141, 20
Beck, J. G. 2000, Sol. Phys., 191, 47
Bouchy, F., & Carrier, F. 2002, A&A, 390, 205
Bouvier, J., Bertout, C., Benz, W., & Mayor, M. 1986, A&A, 165, 110
Carrier, F., & Bourban, G. 2003, A&A, 406, L23
Chaboyer, B., Demarque, P., & Pinsonneault, M. H. 1995, ApJ, 441, 865
Chaplin, W. J., Kjeldsen, H., Bedding, T. R., et al. 2011, ApJ, 732, 54
Charbonneau, P., & MacGregor, K. B. 1993, ApJ, 417, 762
Choi, P. I., & Herbst, W. 1996, AJ, 111, 283
Collier Cameron, A., et al. 2009, MNRAS, 400, 451
Demarque, P., Guenther, D. B., Li, L. H., Mazumdar, A., & Straka, C. W. 2008, Ap&SS, 316, 31
Denissenkov, P. A., Pinsonneault, M., Terndrup, D. M., & Newsham, G. 2010, ApJ, 716, 1269
DeWarf, L. E., Datin, K. M., & Guinan, E. F. 2010, ApJ, 722, 343
Donahue, R. A., Saar, S. H., & Baliunas, S. L. 1996, ApJ, 466, 384
Durney, B. R., & Latour, J. 1978, Geophysical and Astrophysical Fluid Dynamics, 9, 241
Eggenberger, P., Charbonnel, C., Talon, S., et al. 2004, A&A, 417, 235
Endal, A. S., & Sofia, S. 1979, ApJ, 232, 531
Gilliland, R. L., Brown, T. M., Christensen-Dalsgaard, J., et al. 2010, PASP, 122, 131
Gorshanov, D. L., Shakht, N. A., & Kisselev, A. A. 2006, Astrophysics, 49, 386
Haisch, K. E., Jr., Lada, E. A., & Lada, C. J. 2001, ApJ, 553, L153
Hallam, K. L., Altner, B., & Endal, A. S. 1991, ApJ, 372, 610
Hartman, J. D., et al. 2008, ApJ, 675, 1233
Hartman, J. D., et al. 2009, ApJ, 691, 342
Hartman, J. D., Bakos, G. Á., Kovács, G., & Noyes, R. W. 2010, MNRAS, 1162
Hartman, J. D., Bakos, G. Á., Noyes, R. W., Sipőcz, B., Kovács, G., Mazeh, T., Shporer, A., & Pál, A. 2011, AJ, 141, 166
Henderson, C. B., & Stassun, K. G. 2011, arXiv:1112.2211
Herbst, W., Maley, J. A., & Williams, E. C. 2000, AJ, 120, 349
Irwin, J., Aigrain, S., Hodgkin, S., Irwin, M., Bouvier, J., Clarke, C., Hebb, L., & Moraux, E. 2006, MNRAS, 370, 954
Irwin, J., Irwin, M., Aigrain, S., et al. 2007, MNRAS, 375, 1449
Irwin, J., Hodgkin, S., Aigrain, S., Hebb, L., Bouvier, J., Clarke, C., Moraux, E., & Bramich, D. M. 2007, MNRAS, 377, 741
Irwin, J., Hodgkin, S., Aigrain, S., Bouvier, J., Hebb, L., & Moraux, E. 2008, MNRAS, 383, 1588
Irwin, J., Hodgkin, S., Aigrain, S., et al. 2008, MNRAS, 384, 675
Irwin, J., Berta, Z. K., Burke, C. J., et al. 2011, ApJ, 727, 56
Jackson, R. J., & Jeffries, R. D. 2010, MNRAS, 402, 1380
Jay, J. E., Guinan, E. F., Morgan, N. D., Messina, S., & Jassour, D. 1997, Bulletin of the American Astronomical Society, 29, #120.04
Kawaler, S. D. 1988, ApJ, 333, 236
Keppens, R., MacGregor, K. B., & Charbonneau, P. 1995, A&A, 294, 469

Kervella, P., Thévenin, F., Ségransan, D., et al. 2003, A&A, 404, 1087
Kervella, P., Mérand, A., Pichon, B., et al. 2008, A&A, 488, 667
Kim, Y.-C., & Demarque, P. 1996, ApJ, 457, 340
Kiraga, M., & Stepien, K. 2007, Acta Astronomica, 57, 149
Kjeldsen, H., Bedding, T. R., & Christensen-Dalsgaard, J. 2009, IAU Symposium, 253, 309
Koenigl, A. 1991, ApJ, 370, L39
Krishnamurthi, A., Pinsonneault, M. H., Barnes, S., & Sofia, S. 1997, ApJ, 480, 303
Krishnamurthi, A., et al. 1998, ApJ, 493, 914
Lachaume, R., Dominik, C., Lanz, T., & Habing, H. J. 1999, A&A, 348, 897
Luck, R. E., & Heiter, U. 2005, AJ, 129, 1063
Lustig, G. 1983, A&A, 125, 355
MacGregor, K. B., & Brenner, M. 1991, ApJ, 376, 204
Mamajek, E. E. 2009, American Institute of Physics Conference Series, 1158, 3
Mamajek, E. E., & Hillenbrand, L. A. 2008, ApJ, 687, 1264
Meibom, S., Mathieu, R. D., & Stassun, K. G. 2009, ApJ, 695, 679
Meibom, S., Mathieu, R. D., Stassun, K. G., Liebesny, P., & Saar, S. H. 2011, ApJ, 733, 115
Meibom, S., et al. 2011, ApJ, 733, L9
Miglio, A., & Montalbán, J. 2005, A&A, 441, 615
Morel, P. 1997, A&AS, 124, 597
Morel, P., Provost, J., Lebreton, Y., Thévenin, F., & Berthomieu, G. 2000, A&A, 363, 675
Mosser, B., Belkacem, K., Goupil, M.-J., et al. 2010, A&A, 517, A22
Neuforge-Verheecke, C., & Magain, P. 1997, A&A, 328, 261
Noyes, R. W., Hartmann, L. W., Baliunas, S. L., Duncan, D. K., & Vaughan, A. H. 1984, ApJ, 279, 763
Pace, G., & Pasquini, L. 2004, A&A, 426, 1021
Patten, B. M., & Simon, T. 1996, ApJS, 106, 489
Perryman, M. A. C., & ESA 1997, ESA Special Publication, 1200,
Pinsonneault, M. H., Narayanan, V. K., Steigman, G., & Walker, T. P. 1998, Cool Stars, Stellar Systems, and the Sun, 154, 959
Pinsonneault, M. H., Kawaler, S. D., & Demarque, P. 1990, ApJS, 74, 501
Pinsonneault, M. H., Kawaler, S. D., Sofia, S., & Demarque, P. 1989, ApJ, 338, 424
Pizzolato, N., Maggio, A., Micela, G., Sciortino, S., & Ventura, P. 2003, A&A, 397, 147
Pourbaix, D., Nidever, D., McCarthy, C., et al. 2002, A&A, 386, 280
Radick, R. R., Thompson, D. T., Lockwood, G. W., Duncan, D. K., & Baggett, W. E. 1987, ApJ, 321, 459
Rebull, L. M., Wolff, S. C., & Strom, S. E. 2004, AJ, 127, 1029
Reiners, A. 2006, A&A, 446, 267
Reiners, A., & Mohanty, S. 2012, ApJ, 746, 43
Sestito, P., & Randich, S. 2005, A&A, 442, 615
Schou, J., et al. 1998, ApJ, 505, 390
Schwarzenberg-Czerny, A. 1996, ApJ, 460, L107
Shu, F., Najita, J., Ostriker, E., Wilkin, F., Ruden, S., & Lizano, S. 1994, ApJ, 429, 781
Sills, A., Pinsonneault, M. H., & Terndrup, D. M. 2000, ApJ, 534, 335
Skumanich, A. 1972, ApJ, 171, 565
Söderhjelm, S. 1999, A&A, 341, 121
Spada, F., Lanzafame, A. C., Lanza, A. F., Messina, S., & Collier Cameron, A. 2011, arXiv:1105.3125
Stauffer, J. R., Hartmann, L. W., & Jones, B. F. 1989, ApJ, 346, 160
Stepien, K. 1994, A&A, 292, 191
Tinker, J., Pinsonneault, M., & Terndrup, D. 2002, ApJ, 564, 877
van Saders, J. L., & Pinsonneault, M. H. 2012, ApJ, 746, 16
Walker, G. A. H., Walker, A. R., Irwin, A. W., et al. 1995, Icarus, 116, 359
Wilson, O. C. 1963, ApJ, 138, 832
Wolff, S. C., Boesgaard, A. M., & Simon, T. 1986, ApJ, 310, 360